Summer 2017

3D bioprinting a PCL/13-93B3 glass composite and its potential use as a bio-ink

Caroline Blair Murphy

3D BIOPRINTING A PCL/13-93B3 GLASS COMPOSITE AND ITS POTENTIAL USE AS A BIO-INK

By

CAROLINE MURPHY

A THESIS

Presented to the Faculty of the Graduate School of the

MISSOURI UNIVERSITY OF SCIENCE AND TECHNOLOGY

In Partial Fulfillment of the Requirements for the Degree

MASTER OF SCIENCE IN MECHANICAL ENGINEERING

2017

Approved by

Dr. Ming Leu, Co-Advisor
Dr. Julie Semon, Co-Advisor
Dr. Cheng Wang

ABSTRACT

A major limitation of using synthetic scaffolds in tissue engineering is little growth of incorporated cells in the interior of the scaffold, resulting in insufficient angiogenesis in the scaffold interior. Recently, cells have been 3D bioprinted concurrently with biomaterials to produce a cellularized, bioactive, angiogenic 3D environment. This thesis describes a novel solvent-extrusion method for printing polycaprolactone (PCL)/bioactive borate glass composite as a biomaterial for a cell-laden scaffold.

Bioactive borate glass was added to a mixture of PCL and organic solvent to make an extrudable paste, creating scaffolds measuring $10\times10\times1$ mm^3 in overall dimensions with pore sizes ranging from 100–300 μm. We compared depositing hydrogel droplets to depositing hydrogel filaments in between the PCL/borate glass composite filaments. Degradation of the composite scaffold with and without the presence of hydrogel was investigated by soaking the scaffold in cell culture medium. The weight loss of the scaffold together with formation of a hydroxyapatite-like layer on the surface shows the excellent bioactivity of the scaffold. This work demonstrates that incorporating borate glass to increase the angiogenic capacity of the fabricated scaffolds is feasible. We also compared cell survival and viability between the composite bio-ink to two commonly used hydrogels, Matrigel and Pluronic F127. The viability and proliferation of cells in the different biomaterials were analyzed with different methods demonstrating that cell viability was similar between the different bio-inks. This 3D bioprinting method shows a high potential to create a bioactive, highly angiogenic 3D environment required for complex and dynamic interactions that govern the cell's behavior *in vivo*.

ACKNOWLEDGMENTS

The author wishes to thank MO-SCI Corporation (Rolla, Missouri, USA) for providing the glass used in these studies. The author also wishes to thank the undergraduate students involved in this research: Mariahe Long and Jakeb Baldridge for their assistance printing and imaging.

The author extends thanks to Dr. Krishna Kolan for his invaluable help with all aspects of the project from the very beginning. Gratitude is also extended to Richard Watters for his training and assistance with isolation of rat cells and histology.

The author would also like to thank the committee members – Drs. Julie Semon, Ming Leu, and Cheng Wang – for their advice and guidance.

TABLE OF CONTENTS

LIST OF FIGURES

Page

LIST OF TABLES

Page

LIST OF ABBREVIATIONS

Abbreviation	Description
αMEM	Minimum essential media alpha modified
ASC	Adipose derived MSC
BMSC	Bone marrow derived MSC
CCM	Complete culture media
CF	Chloroform
D-10	Rat culture media
DMEM	Dubelcco's minimum essential media
FBS	Fetal bovine serum
FDM	Fused deposition modeling
HA	Hydroxyapatite
MSC	Mesenchymal stem cell
PBS	Phosphate buffered saline
PCL	Polycaprolactone
SVF	Stromal vascular fraction
13-93B3	Borate based bioactive glass
45S5	Silicate based bioactive glass

1. INTRODUCTION

Bone defects, resulting from trauma, cancer, arthritis, infection, or congenital skeletal abnormalities, account for approximately 34 million surgeries per year.[1] While autologous bone grafts achieve the best result, they create new defects and the possibility of increased morbidity in donors.[2–6] Allografts can circumvent these issues, but they are troubled with limited availability, concerns over immunogenicity, and potential disease transmission.[7] Engineered bone scaffolds are another treatment option but have not been as successful as autologous grafts due to insufficient vascularization and poor biomechanical function.[8–10]

Additive manufacturing, also known as 3D bioprinting, is of particular interest in orthopedics due to the ability to print scaffolds with complex designs, controlled chemistry, and interconnected pores. 3D bioprinting is a process that fabricates a "living" construct in a layer-by-layer fashion using a "bio-ink" (cells suspended in a medium) with or without additional materials. The creation of a 3D environment with spatial arrangement of cells and materials is essential for vascularization and, therefore, complete implant integration with the surrounding tissue.

3D bioprinting techniques can be broadly classified into four categories: (i) laser-assisted,[11,12] (ii) inkjet-based,[13] (iii) stereolithography,[10] and (iv) extrusion-based printing.[14] In laser-assisted printing, energy generated by a laser pulse is used indirectly to create a droplet from a cell containing ribbon that is then deposited on a substrate.[8,9] The advantage of this process is being able to print relatively high viscosity biological materials with suspended cells. However, process precision and material properties required for shape control limits the availability of materials for this system. Inkjet printing produces fine droplets of cells suspended in media that can be deposited at high resolutions (~20 μm). However, the process can only utilize low-viscosity materials.[6,7] Stereolithography is a well-known and established technique in the 3D printing industry and works on the principle of selective photopolymerization using a light energy source on a reservoir containing materials and cells with a photo initiator. The resolution of the process depends on the laser spot-size which is generally high but is limited to using only photopolymerizable materials.[10]

The last category of bioprinting, extrusion-based 3D bioprinting, allows the printing of cells, hydrogels, and other materials using one or multiple syringes and a pressure system. The pressure system consists of either a mechanical piston or a pneumatic pressure source (mostly compressed air) that is computer controlled. The material is extruded through a nozzle tip (industry standard) with orifice ranging from less than 100 μm to several hundred microns in diameter. The main advantage of extrusion based bioprinting is the wide range of materials that are compatible with the process, including high viscosity biopolymer pastes and hydrogels. The process can deposit hydrogels with different gelation mechanisms, with high cell density, and with minimal waste in comparison to laser assisted and stereolithography techniques. Overall, extrusion-based bioprinting is a very promising biofabrication method.[15,16]

Synthetic materials, such as polycaprolactone (PCL), provide strength and elasticity to scaffolds. In addition, due to the high temperature required to melt other biopolymers such as polylactic acid (PLA, with a melting point of 160^{o}C), PCL has become one of the most widely used biocompatible polymers owing to its low melting point of 60^{o}C.[17,18] For 3D printing, PCL is an attractive option because of its good rheological and viscoelastic properties. Despite its slow degradation rate (~2 years depending on the molecular weight), PCL has been widely used to fabricate scaffolds for bone tissue engineering.[18–20]

Because pure polymer scaffolds fabricated using the melt-deposition process are only biocompatible and do not react in the body, another challenge is to make the scaffold bioactive. Bioactive glasses are biocompatible and resorbable, can be made into custom compositions and geometries, can be tailored to reliably degrade in minutes to years, and can be doped with most elements (i.e. copper).[12] Additionally, most bioactive glasses form a hydroxyapatite (HA)-like layer, which is the precursor to bone, that bonds with both hard and soft tissue.[9] Recently, silicate bioglasses – such as 45S5 – have been shown to be non-toxic to stem cells, serve as an excellent delivery vehicle for angiogenic factors and cells, and can contribute to stem cell differentiation into an osteogenic lineage.[21,22] However, less is known about the effect of borate based bioglass 12-93B3. 13-93B3 bioglass has a higher reaction rate (5-10 times faster than silicate glasses); is more resorbable (60 to 70% wt. loss) in a few days to weeks; and is angiogenic,

antimicrobial, and osteo stimulatory/conductive (Table 1.1).[23–25] Despite these promising attributes, the use of borate based bioglass is limited due to the low strength and brittleness of glass in porous scaffolds required for bone repair.

Table 1.1 Composition of 45S5 and 13-93B3 bioactive glasses.[14]

Glass	SiO_2	B_2O_3	Na_2O	K_2O	MgO	CaO	P_2O_5	*In vivo* Reaction rate (μm/wk)
45S5	45.0	0	24.5	0	0	24.5	6.0	~5-6
13-93B3	0	53.0	6.0	12.0	5.0	20.0	4.0	~30-45

Composite scaffolds can combine the benefits of multiple materials. By increasing the complexity of the scaffold with multiple materials and cells, matching both the biomechanical and biological properties of the target tissue becomes more feasible.[15,16] In the past, researchers made polymer-bioactive glass scaffolds using fused deposition modeling (FDM).[26] In FDM, the polymer is melted and deposited as filaments that solidify upon cooling in a layer-by-layer fashion. However, no significant improvement in bioactivity and cell growth was reported, which could be due to the inadequate ionic dissolution of the glass into the surrounding environment. This makes melt-deposition options unattractive for fabrication of polymer-glass composite scaffolds as they are less reactive when combined with bioactive materials. Therefore, it is essential to investigate alternate approaches for printing materials, such as solvent-based fabrication methods.

A variety of solvents are available to dissolve different biopolymers.[27] Extrusion of solvent dissolved polymer and bioactive glass is safe at room temperature and reduces the process complexity since there is no need for temperature control. This method can be adopted by most of the existing open-source 3D printers available in the market. Previous studies have used chloroform (CF) to dissolve PCL for biomaterial applications.[28] As a

solvent, CF provides: (i) a high viscosity paste, making it suitable for extrusion-based 3D printing, (ii) fast evaporation (~2 min), making it safe to print cells during the fabrication process, (iii) filament porosity for accelerated glass dissolution to the surrounding, and (iv) faster polymer bulk degradation by exposing the interior of filament.

Another requirement to fabricate a "living" construct is cells. Mesenchymal stem / progenitor cells (MSCs) have been used for cell therapy and in tissue engineering because of their ability to differentiate into multiple mesenchymal lineages *in vitro*, immune modulatory effects, and angiogenic capacity.[29,30] MSCs have been isolated from several tissues, including the bone marrow (BMSCs), adipose tissue (ASCs), and skin tissue.[31–34] The frequency of MSCs in adipose tissue is much higher than the more commonly studied source of bone marrow, yielding 100 to 500 times more cells per tissue volume.[35,36] ASCs have similar self-renewal abilities, common surface epitopes, growth kinetics, and cytokine expression profiles to BMSCs. ASCs are isolated from the stromal vascular fractions (SVF) of subcutaneous white adipose tissue. A heterogenous cell population, SVF also includes blood cells, endothelial cells, adipocytes, macrophages, and various growth factors.[37–40]

In this series of studies, we (i) developed a novel composite scaffold wherein a polymer is dissolved in chloroform, mixed with borate bioactive glass, and then extruded to fabricate the scaffold, (ii) used this novel composite as a bio-ink for stem cells and compared cell survival to other commonly used bio-inks, (iii) compared different sources of stem cell populations from different species as bio-printing candidates, (iv) investigated the best scientific method to analyze stem cell activity after printing cells in different bio-inks.

2. MATERIALS AND METHODS

2.1. CELL CULTURE

2.1.1. Isolation of Rat Stromal Vascular Fraction. Subcutaneous white adipose tissue was collected from 6-13 week old Sprague Dawley rats weighing 180-250 grams. Approximately 3.5 grams of adipose tissue was collected per rat. Adipose tissue was washed in 50 mL of Hanks' balanced salt solution (HBSS, Lonza, Walkersville, MD, USA) 2-3 times until the medium remained clear when shaken vigorously. To isolate the stromal vascular fraction (SVF), adipose tissue was minced with a razorblade and then incubated in a 0.1% (w/v) collagenase (from Clostridium histolyticum, Sigma-Aldrich, St. Louis, MO) HBSS solution in a 50 mL centrifuge tube at 37°C on a 5x G shaker (Innova 4000, New Brunswick Scientific, Edison, NJ) for approximately 3 hours. During incubation, tissue was additionally shaken manually and vigorously for 5-10 seconds every 15 minutes.

After forming a "soup like" consistency, the collagenase was neutralized by adding an equal volume of D-10 cell culture media that consisted of 10% fetal bovine serum (FBS, Corning, Manassas, Virginia, USA), 1% 100x L-glutamine (GE Life Sciences, Logan, UT), 2% 100x antibiotic/antimycotic (GE Life Sciences, Logan, UT) and Dubelcco's minimum essential media (DMEM, Sigma-Aldrich, St. Louis, MO). Digested tissue was filtered through a 100 μm mesh filter followed by a 70 μm mesh filter. The filtered cell solution was centrifuged at room temperature at 1000x g for 10 minutes. The supernatant was aspirated, leaving the SVF pellet.

2.1.2. Isolation of Rat Bone Marrow Derived Mesenchymal Stem Cells. Femurs were collected from 6-13 week old Sprague Dawley rats averaging 180-250 grams. Within one hour of being sacrificed with carbon dioxide, femurs were removed, both distal ends of the femur were cut, and an 18 gauge needle was inserted into the shaft. Approximately 5 mLs of D-10 media was expelled into the femur to flush cells into a 25 cm^2 culture flask (TPP, Trasadingen, Switzerland). Flushing was repeated 3-5 times. After cells incubated overnight at 37°C with 5% CO_2, they were then washed three times with 2 mL of pre-warmed phosphate buffered saline (PBS; Lonzo, Walkersville, MD). D-

10 media was replaced every 3-4 days. When cells became 65-75% confluent, flasks were washed three times with 2 mL of pre-warmed PBS, harvested with 0.25% trypsin/ 1mM EDTA, and passaged at 100 cells/ cm^2. Passage 2-4 was used for all experiments.

2.1.3. Cell Culture of Human Mesenchymal Stem Cells. Frozen vials of approximately $1x10^6$ human ASCs (hASCs; LaCell, New Orleans, LA) or human BMSCs (hBMSCs; Texas A&M Institute for Regenerative Medicine, Temple, TX) were obtained from separate donors (Table *2.1*). Vials were quickly unthawed in a water bath, plated on 150 cm^2 culture dishes in 25 mL complete culture media (CCM), and incubated at 37ºC with 5% CO_2 overnight. CCM contained 10% fetal bovine serum, 1% 100x L-glutamine, 2% 100x antibiotic/antimycotic, and minimum essential medium alpha modified (α-MEM, Sigma-Aldrich, St. Louis, MO). Cells were washed three times with 4 mL of pre-warmed PBS, harvested with 0.25% trypsin/ 1mM EDTA, and passaged at 100 cells/cm2 in CCM. Media was changed every 3 to 4 days. For all experiments, sub-confluent cells (≤70% confluent) between passages 2 and 6 were used.

Table 2.1 Demographic information for human MSCs.

Cell Type	Race	Age	Gender	BMI
hASC-1	Caucasian	40	F	24.37
hASC-2	Caucasian	49	F	27.34
hASC-3	Caucasion	28	F	24.65
hBMSC-1	N/A	28	M	N/A

2.2. PREPARATION OF BIO-INKS

2.2.1. PCL/13-93B3 Composite. Polycaprolactone (Sigma- Aldrich, St. St. Louis, MO) was dissolved in chloroform (CF; Sigma-Aldrich, St. Louis, MO) in a covered glass container with the help of a stirrer at ~45°C. The PCL weight to CF volume

ratio (grams:mL) was varied from 1:1 to 5:4 to determine the ideal ratio for printing. An appropriate ratio was established by visually inspecting the paste and through filament extrusion using a digital syringe dispenser (Loctite®, Henkel North America, Rocky Hill, CT). Then, 13-93B3 glass (Mo-Sci Corporation, Rolla, MO) with ~20 µm particle size was added to the PCL:CF mix in five different weight percentages in increments of 10% ranging from 10% to 50%. A magnetic stir bar was used to uniformly mix the composite paste, and no settling of the glass particle precipitate was observed before transferring the paste to a syringe. Each ratio was tested using a digital syringe dispenser at air pressure ranging from 10 to 50 psi and with nozzle tip diameter ranging from 110 to 600 µm.

2.2.2. Matrigel. Matrigel (Corning, Bedford, MA) was thawed on ice for 3 hours and diluted in DMEM to 9 mg/mL for droplets or to 4.5 mg/mL for filaments. For droplets, hASCs were suspended at a concentration of $10x10^6$/mL of Matrigel. For filaments, $5x10^6$ rBMSCs/mL or $5x10^6$ rSVF/mL of Matrigel was used. Matrigel was gently mixed to obtain a uniform distribution of cells and transferred to a 160 µm nozzle tip. Matrigel incubated at 37°C for 5 minutes to crosslink before printing.

2.2.3. Pluronic F-127 Hydrogel. Pluronic F-127 hyrdogel (Pluronic; Sigma-Aldrich, St. Louis, MO) of 15% or 25% (w/v) was prepared using DMEM in a 50 mL glass beaker placed in an ice bath. The solution was mixed, covered, using a magnetic stir bar until Pluronic dissolved (about 30 minutes). The solution was allowed to sit for an hour at 4°C to remove bubbles formed during stirring. For filaments, $5x10^6$ rBMSCs/mL or $5x10^6$ rSVF/mL of Pluronic was used. Pluronic was gently mixed to obtain a uniform distribution of cells and transferred to a 160 µm nozzle tip. The Pluronic incubated at 37°C for 5 minutes to crosslink before printing.

2.3. SCAFFOLD FABRICATION

Scaffolds ($10x10\ mm^2$) were printed with 0-90° orientation of the filaments in alternate layers. Printing was performed with an assembled DIY 3D printer (Geeetech, Prusa I3 A Pro) that was modified to have two syringes connected to digital dispensers that were computer controlled (Figure 2.1). Scaffolds were printed either on a microscope slide (Thermo Fischer Scientific, Rochester, NY) or in a 12-well tissue culture plate (TPP,

Trasadingen, Switzerland). The printing parameters such as filament spacing, layer height, printing speed, etc. were identified based on visual inspection and optical microscopic images after a single layer extrusion. Printing parameters such as needle tip sizes and printing speed were uniform for all paste compositions after initial trials. Parameters such as air pressure and filament overlap were correspondingly modified for different pastes (Table *3.1*).

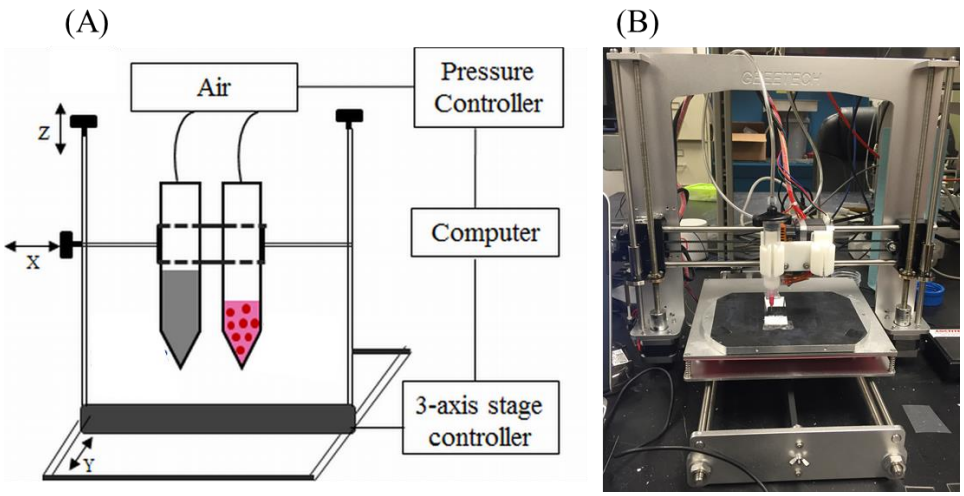

Figure 2.1 Schematic of (A) printer design and (B) set-up.

2.4. SCAFFOLD DEGRADATION

Degradation of the PCL/13-93B3 composite was evaluated on 10x10x1 mm^3 scaffolds. Scaffolds were weighed and then placed in high density polyethylene (HDPE) bottles containing 300 mL of α-MEM per 1 g of scaffold for soaking, and incubated at 37^{o}C from 1-14 days. After incubation, scaffolds were removed, gently washed with 2 mL of room temperature deionized (DI) water three times, and dried overnight. The dried scaffold was weighed to calculate the weight loss percentage. Each time interval had an n=3 and results were reported as mean ± standard deviation using a student t-test.

2.5. SCAFFOLD CHARACTERIZATION

Microscopic images were used to measure the filament width and pore size of the PCL/13-93B3 composite. Once fully dried, samples of the scaffold both just after printing and after the degradation study were sputter coated with gold/palladium (Au/Pd) for 60 seconds. Scanning electron microscopy (SEM, Hitachi S-4700 FESEM, Hitachi Co., Tokyo, Japan) images were taken to evaluate the surface morphology of the scaffolds, internal structure of the filaments, and formation of hydroxyapatite-like material on the scaffold surface. Scans were run from 2θ values ranging from 10º to 80º using Cu Kα radiation (λ = 0.154056 nm) for X-ray diffraction (XRD) analysis (Philips X-Pert, Westborough, MA) on the as-received PCL, as-printed PCL/B3 glass scaffold, and the scaffold after α-MEM immersion to determine the changes in the crystalline/amorphous nature of the material. At least five measurements were taken of each scaffold; results were reported as mean ± standard deviation

2.6. LIVE/DEAD ASSAY

Printed cell-laded scaffolds incubated for 1 or 7 days in D-10 at 37ºC with 5% CO_2. Cell numbers and viability was evaluated by a live/dead assay, per manufacturer's protocol (Life Technologies, Eugene, OR). In brief, scaffolds were removed from the incubator, washed three times in pre-warmed PBS, and incubated in live/dead stain for 15 minutes at room temp. Five images per scaffold were taken on a fluorescent microscope (Olympus IX51, Melville, NY), and images were quantified using Fiji software (NIH, Betheseda, MD). Each time point had an n=3 and results were reported as mean ± standard deviation using a student t-test

2.7. DNA QUANTIFICATION

Printed cell-laded scaffolds incubated for 1 or 7 days in D-10 at 37ºC with 5% CO^2. DNA was quantified with CyQuant, per manufacturer's protocol (Life Technologies, Eugene, OR). In brief, scaffolds were removed from the incubator, washed three times in pre-warmed PBS, lifted with 0.25% trypsin/1mM EDTA, pelleted

in a 1.5 mL vial, and frozen at -80°C. The pellet was incubated with CyQuant at room temperature for 5 minutes and fluorescence was measured at a wavelength of 480 nm using a microplate reader (FLUOstar Omega, BMG Labtech, Offenburg, Germany). The mean cell number ± standard deviation was calculated in excel with n=3 against a standard with a curve fit of R=0.99 and graphed.

2.8. QUANTIFICATION OF CELL NUMBER

To determine the number of cells printed, droplets of bio-ink were printed on a microscope slide and immediately fixed in 10% paraformaldehyde (PFA; Affymetrix, Cleveland, OH). Droplets were stained with DAPI (Vector Laboratories, Burlingame, CA) and examined using a fluorescent microscope. The entire area of each droplet (n=4) was imaged and the approximate cell number was determined using Fiji software.

2.9. METABOLIC QUANTIFICATION

Printed cell-laded scaffolds incubated for 1 or 7 days in D-10 at 37°C with 5% CO^2. Scaffolds were then removed from the incubator, washed three times with PBS, lifted with 0.25% trypsin/1mM EDTA, and pelleted in a 1.5 mL vial.

Cells were re-suspended in 100 µL of D-10, transferred to a 96-well culture plate (TPP, Trasadingen, Switzerland) and cellular metabolic activity was measured with an MTT assay (Trevigen, Gaithersburg, MD) performed according to manufacturer's protocol. Briefly, the MTT reagent was added, the plate incubated for 3 hours at 37°C, detergent was added, and the plate was left covered at room temperature overnight. Absorbance was measured at a wavelength of 570 nm using a microplate reader. Cell viability was calculated with n=3 using Excel and the mean absorbance ± standard deviation was graphed.

3. RESULTS

3.1. FABRICATION OF NOVEL PCL/13-93B3 GLASS SCAFFOLD

3.1.1. Single Layer Tests. The weight percentage of PCL was varied from 1:1 to 5:4 (in grams of PCL to mL of chloroform) to determine the best ratio for fabricating the scaffold. During the initial set of tests, different compositions of paste were extruded using a hand-held syringe and with the help of a digital dispenser while varying the nozzle tip size and the air pressure. An air pressure between 30 and 50 psi provided uniform extrusion of the PCL+chloroform mixture. The ideal ratio of PCL and chloroform was determined to be 5 g of PCL to 3 mL of chloroform, extruded at 30 psi using a 260 µm (25G) nozzle tip. A larger tip size (>260 µm) would result in thick filaments which were not beneficial for achieving small pore size distribution in the scaffold. From there, 10 wt.% 13-93B3 glass was mixed with the PCL and chloroform and extruded using the printer from 3 to 10 mm/s. A reduced filament width (from 0.8 mm to 1.8 mm) can be observed with increasing printing speed (Figure 3.1). The width of the filament also depended on the homogeneity of the mixture.

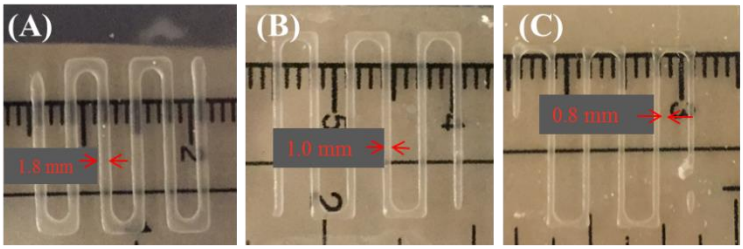

Figure 3.1 Single layer tests with C1 composite using different printing speeds (A) 3mm/s, (B) 5mm/s, and (C) 10 mm/s.

3.1.2. Two Layer Tests. The filament height and the spacing of the first layer were crucial parameters when printing successive layers. The filament height determined the height for each layer while the filament spacing defines how well the filaments bridge across the previous layer. The average height of filaments printed using a speed of 8 mm/s was ~75 µm (Figure 3.2A). Therefore, a distance of 100 µm between the nozzle tip and substrate or previously deposited layer was used to fabricate subsequent scaffolds. The height of the filaments for 40 wt% and 50 wt% glass compositions remained the same if the same nozzle tip was used. The roundness of the filament improved with a smaller tip but because of the nozzle clogging issues, all the experiments were carried out with a 260 µm tip. Another important factor in this study is the dwell time between consecutive layers as this allows the chloroform to evaporate and allow the bottom layer to become more solid. A longer dwell time (>5 min) would warp the layer and a shorter dwell time (<1 min) is not sufficient for the layer to dry. The difficulty in bridging the second layer without dwell time can be noticed and was substantially improved with 1 mm dwell time (Figure 3.2C). The ideal dwell time between layers was determined to be 2-3 minutes (Figure 3.2D).

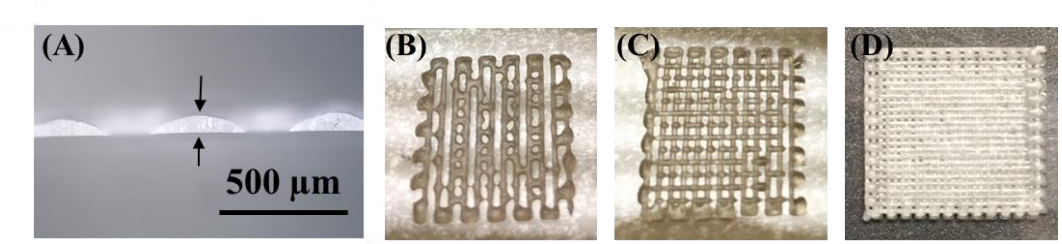

Figure 3.2 Determining layer height and dwell time on 10x10 mm^2 scaffolds. (A) Cross-sectional view of the C3 filament measuring ~75 µm in height, (B) Second layer printing with zero dwell time, (C) Second layer printing with 1 min dwell time, and (D) Second layer printed with 2.5 min dwell time

3.1.3. Multiple Layer Scaffolds. Based on the previous tests, scaffolds with multiple layers were fabricated using all five compositions (i.e. 10 wt.% to 50 wt.% 13-93B3 glass). The minimum air pressure required to extrude the paste increased when glass content was increased from 10 wt.% to 30 wt.%. At higher glass content (40 wt.% and 50 wt.%), the nozzle clogged during fabrication. Therefore, additional chloroform (about 1 mL) was added to the paste to reduce the viscosity for clog-free extrusion using the 260 µm tip. The 13-93B3 glass weight percentage and PCL:Chloroform ratios used to make composite pastes are shown in Table 3.1.

Table 3.1 PCL/13-93B3 paste compositions and printing parameters.

Composite Paste #	13-93B3 Glass (Wt. %)	Air Pressure (psi)	Filament Spacing (µm)	PCL:CF (g to mL)	Final Printing Parameters (using C5 paste)
C1	10	30	600-800	5:3	Printing speed – 8 mm/s
C2	20	30	600-800	5:3	Dwell time – 2 min
C3	30	40	600-800	5:3	Nozzle distance – 100 µm
C4	40	30	700-800	5:4	Air pressure – 30 psi
C5	50	30	700-800	5:4	Nozzle tip – 260 µm

A filament width of 397±10 µm was measured for scaffolds printed with the C5 paste while average pore size is dependent on the filament spacing. A filament spacing of 600 µm provided square pores measuring ~160 µm (Figure 3.3A). In comparison, the average pore size was ~350 µm for scaffolds with 800 µm filament spacing while in scaffolds with a spacing 700 µm, the pore size varied from ~200 to ~300 µm. Therefore, pore sizes could be adjusted by modifying the filament spacing, to a certain extent, to suit a certain tissue engineering application of the fabricated scaffold.

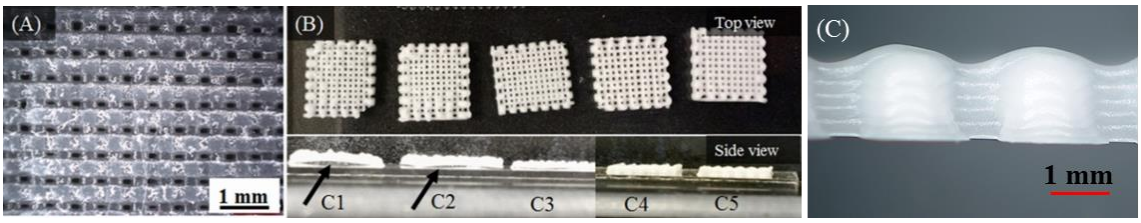

Figure 3.3 Micro- and macroscopic images of PCL/13-93B3 composite scaffolds. (A) Optical microscopic image showing the pores (~160 µm) in a composite scaffold fabricated with C5 paste. (B) Scaffolds fabricated with different composite pastes (C1 to C5); warpage shown with an arrow indicating space between scaffold and slide. Warpage was minimal in C3/C4 scaffolds and completely absent in C5 scaffolds. (C) Cross section of C5 scaffold showing filaments unable to bridge filaments from previous layer.

It should be noted that the maximum thickness (or height) of the scaffolds depends on the degree of chloroform evaporation and the distance between layers. All the experiments were carried out at room temperature (64°F) where the variation in relative humidity (58-60%) was not considered to be a major factor. Faster chloroform evaporation would produce warpage of the fabricated scaffold, especially with some dwell time between the layers. Non-uniform distribution of the PCL and glass is not believed to be one of the major factors of warpage as, upon examination of the filaments' microstructure when printed with the same syringe at different time intervals, there was similar and uniform deposition of glass particles throughout the matrix. Therefore, the chloroform evaporation and the percentage of PCL in the composite are two of the crucial factors that determine the warpage. Increasing the glass content in the composite would indirectly decrease the chloroform content and thereby aids in faster evaporation and improves the filament rigidity. Warping was predominant with C1 and C2 pastes while fabricating scaffolds using an 800 µm filament spacing and this led to difficulty in printing after about 8 layers (640 µm) (Figure 3.3B). The warpage in scaffolds fabricated with C3 paste was less pronounced and a scaffold height of 800 µm (10 layers) was obtained. Overall, the best results were achieved for scaffolds fabricated with C5 paste as they were successfully printed to 1 mm height (12 layers). The scaffolds fabricated with C5 paste had enough strength to be safely handled for subsequent degradation and *in vitro* assessment. The scaffolds fabricated with the C3-C5 pastes were reproducible to the

extent that 3 out of 4 scaffolds were consistent in quality. However, even with the C5 paste, there was insufficient bridging between the filaments, resulting in a mesh with pores only in one direction rather than a porous scaffold (Figure 3.3C).

3.2. MICROSCTRUCTURE EVALUATION OF PCL/13-93B3 COMPOSITE SCAFFOLD

Scanning electron micrographs of composite scaffolds made with C4 and C5 composites showed the surface morphology of the filament (Figure *3.4*). Glass particles are conspicuously absent from the surface of the scaffold filaments (Figure *3.4*A-C). No pores on the filament surface were detected even when observed at a 2000x magnification (Figure *3.4*C). Glass particles dispersed in the PCL matrix can be seen in the interior when examining the cross-sectional surface of the filament (Figure *3.4*D-F). The dissolved PCL in chloroform encloses the glass particles and surface tension effects between the nozzle tip and PCL during extrusion appear to have caused the presence of only PCL on the surface.

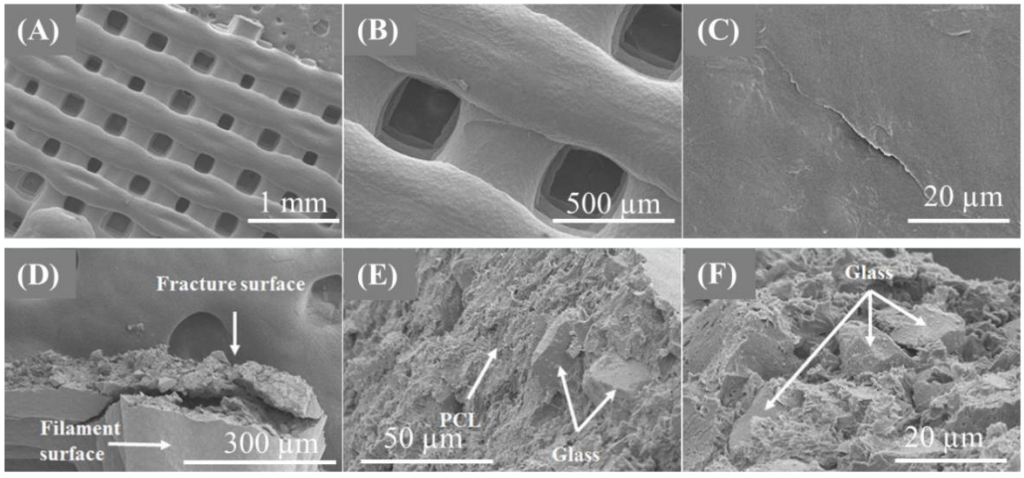

Figure 3.4 SEM images of the C5 PCL/13-93B3 glass scaffold.
(A) Low magnification (30x) and (B) Medium magnification (90x) images of scaffold surface showing filaments and pores, (C) Smooth surface morphology of filament (2000x magnified image), (D) Fractured surface of a broken filament with PCL matrix and glass particles, (E-F) Magnified image of the fracture surface in (D).

3.3. DEGRADATION AND BIOACTIVITY OF PCL/13-93B3 COMPOSITE SCAFFOLD

The degradation of the composite was evaluated by soaking the scaffolds in α-MEM for 1, 3, 7, and 14 days. The scaffold weight before and after immersion (post drying) was recorded at each time interval. No significant weight loss was observed for 3 days (less than 1%), and the measured weight loss was 10.7±5% at 7 days and 23.2±4% at 14 days. As PCL takes a longer time to degrade, the weight loss measured is most likely due to the ionic dissolution of the 13-93B3 borate glass.

Formation of flower like florets, which typically represent HA-like material, was observed on the filament surface (Figure 3.5A and 3.5B). Fine cracks on the filament surface which are a couple of microns wide and up to ten microns or more in length can be observed in Figure 3.5C.

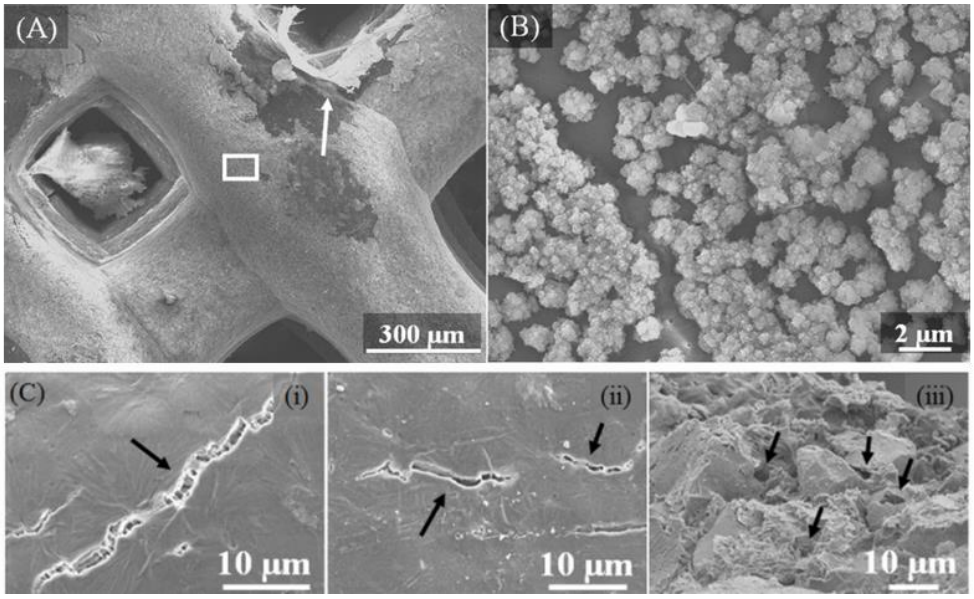

Figure 3.5 SEM images of a C5 glass scaffold after 14 day immersion in α-MEM at 37°C. (A) ~1 µm thick layer was formed on the filament surface (a piece of the reacted layer indicated by arrow raised to expose the polymer beneath), (B) magnified image (8000x) of the area marked in (A) showing the formation of HA-like florets on the filament. (C) Surface cracks on the filament indicated by arrows in (i) and (ii). Pores inside the filament measuring less than 10 µm are indicated by arrows in (iii).

The degradation results also show a controlled release of 13-93B3 glass over a period of two weeks into the surrounding solution (Figure 3.6). In the past, composite thin films have been made using PCL/13-93B3 glass and PCL/45S5 glass with different amount of glass content[28]. The degradation data of such thin films indicate that the entire glass almost completely dissolves in about three days. The graph shown Figure 3.6 compares the weight loss percentage of the PCL/13-93B3 glass thin films (80 µm) with that of the current study. Almost all the 13-93B3 glass was reacted in about 3 days from thin films. The faster degradation in composite films could be due to the small thickness of the film. The scaffolds in the current study are made by filaments which are about 400 µm in diameter and have no surface pores, which explains the very little glass dissolution in three days. However, the water absorbing potential of polymers in general was reportedly found to improve after the addition of bioceramic filler materials such as HA and even bioactive glass[19].

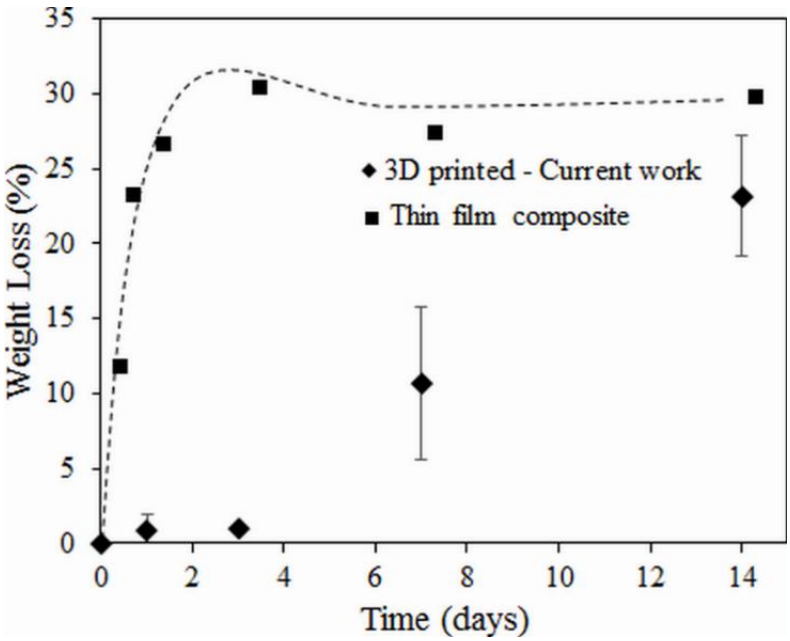

Figure 3.6 Weight loss comparison of 3D printed C5 scaffolds vs. thin film composites.[28] The thickness of the scaffold filaments affects the degradation of the glass.

In this study, the glass dissolution increased significantly after 7 and 14 days, which is believed to be due to the internal porosity of the filament created after the CF evaporation and glass dissolution creating more porosity. The B_2O_3 present in the borate glass (Table 1.1) completely dissolves into the surrounding environment, and the remaining oxides with the exception of MgO participate in the formation of HA. By neglecting the weight of HA formed, it can be theoretically calculated that there is about ~35% weight loss for the scaffold, assuming a complete 13-93B3 glass dissolution in 50:50 PCL/13-93B3 composite. In this study, the weight loss for 50:50 PCL/13-93B3 composite scaffold was ~23%, indicating that ~70% of the 13-93B3 glass present in the scaffold had reacted in 14 days. This degradation vs. time characteristic can be used to develop a controlled degradation of 3D scaffold by adjusting the filament thickness that is beneficial in certain tissue engineering applications, especially in drug delivery.

The energy-dispersive X-ray spectroscopy (EDX) analysis indicated the presence of calcium (Ca), phosphorous (P), and oxygen (O) on the reacted surface of the scaffold after 14-day immersion in α-MEM (Figure 3.7A) by detecting changes in elemental composition in atomic weight percent along a line. The location of the scan was selected such that a scan line (~70 µm long) had to start on a reacted surface, pass through the exposed PCL surface, and end on the reacted surface (Figure 3.7B). All the signals from the EDX analysis correspond to K series emissions (K_α and K_β). It can be observed that the percentage of Ca and P drops to zero along with a decrease in O when scanning the PCL surface (from ~30 µm to ~50 µm in Figure 3.7A). The presence of Ca, P, and O indicates that the glass has reacted and formed a material with a similar profile to HA on the scaffold surface.

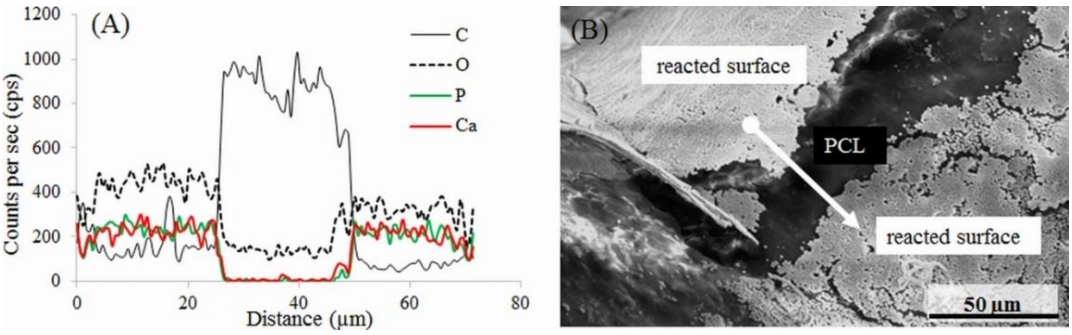

Figure 3.7 EDX analysis on the surface of the C5 scaffold soaked in α-MEM. (A) Graph of line scan data showing the variation in Ca, P, O, and C in atomic weight percentages; presence of Ca, P, and O on the reacted surface confirms the glass reaction and formation of HA-like material, (B) SEM image with the arrow line indicating the scanned area for EDX analysis.

The reacted layer formed on the scaffold surface was ~1 µm thick and not completely uniform (dense collection of florets can be seen in Figure 3.5B). XRD analysis was performed to confirm the presence of crystalline HA but the XRD pattern obtained on a 14 day soaked scaffold could not match the known HA crystalline peak. This is believed to be due to the formation of amorphous HA or non-stoichiometric HA, which is not uncommon in such cases. XRD patterns of the as-received 13-93B3 glass, PCL/13-93B3 glass composite scaffold, and the composite scaffold after soaking in α-MEM for 2 weeks were obtained (Figure 3.8). The semi-crystalline nature of the PCL was confirmed with characteristic peaks (marked by *) and amorphous profile of 13-93B3 glass with no sharp peaks and characteristic hump can be observed in the XRD patterns (Figure 3.8). There are additional peaks observed for the α-MEM soaked sample which could not be identified to a known material in the database (marked by †) that is most likely non-stoichiometric HA. However, the typical amorphous hump seen in glass was not existent in the soaked sample, indicating that most of the 13-93B3 glass in the scaffold had reacted after 14 days.

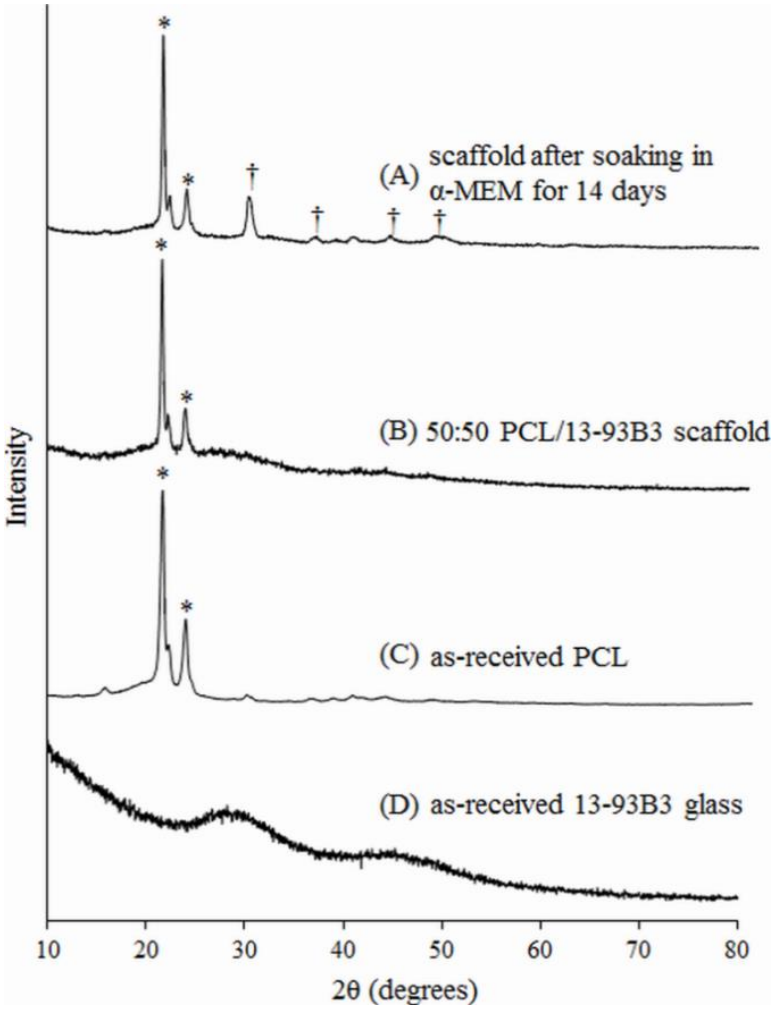

Figure 3.8 XRD patterns comparing different aspects of C5 scaffolds. (A) 50:50 PCL/13-93B3 glass composite scaffold soaked in α-MEM for 14 days, (B) PCL/13-93B3 glass scaffold as printed, (C) as-received PCL showing a semi-crystalline nature with characteristic peaks marked by *, and (D) as-received 13-93B3 glass with characteristic amorphous hump (25° to 35° and 40° to 50°).

3.4. COMPARISON WITH 45S5

Due to the mesh structure seen when using the 13-93B3 glass, a comparison was made using the silicate based 45S5 glass. The printing parameters in Table 3.1 were found to be compatible for a PCL/45S5 composite (Figure 3.9) as well. The average pore size for all compositions was ~360 µm with a filament spacing of 800 µm (Figure 3.9A), similar to the 13-93B3 composite (Figure 3.3A). A common feature of both the 13-93B3

and the 45S5 composite is the filaments filling in the pore space rather than bridging them. In both cases, the result is a mesh structure with pores only in the z-direction rather than a true scaffold (Figure 3.3C and 3.9C). This indicated that the mesh structure was a product of the printing process rather than the glass composition.

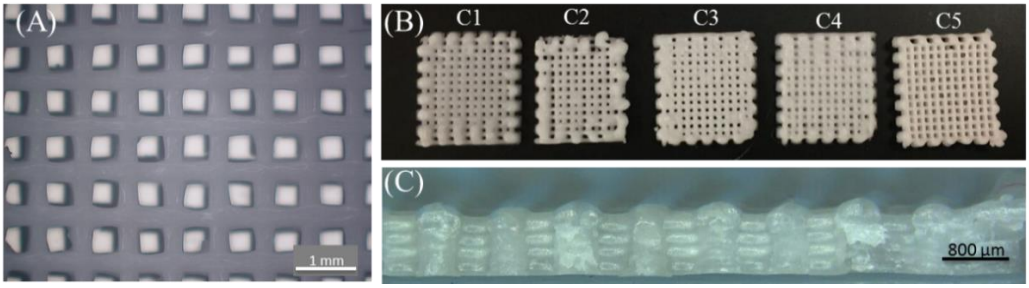

Figure 3.9 Micro- and macroscopic images of PCL/45S5 composite scaffolds. (A) Optical microscopic image showing the pores (~160 µm) in a composite scaffold fabricated with C5 paste. (B) Scaffolds fabricated with different composite pastes (C1 to C5). (C) Cross section of C5 scaffold.

3.5. PRINTING STEM CELLS IN MATRIGEL

3.5.1. Matrigel Droplets. Initially, experiments were conducted to print droplets of hASCs suspended in DMEM. It was determined that a 110 µm (32G) nozzle tip extruded droplets less than 500 µm, which was suitable for printing either on top or alongside the deposited PCL/glass filaments, allowing the printing of the Matrigel to not interfere with the printing of the composite. However, DMEM droplets evaporated too quickly, drying out the cells. Therefore, the option of using a hydrogel, Matrigel, as a medium to suspend the hASCs was examined. The initial set of experiments included dispensing the Matrigel droplets without cells with the syringe dispensing system set-up to determine an appropriate concentration of Matrigel in DMEM and droplet size. A concentration of 10mg/mL Matrigel provided smaller drops (~100 µm), while 8 mg/mL

Matrigel produced larger drops (~500 µm), and 4 mg/mL Matrigel produced even larger drops (1 mm) (Figure 3.10).

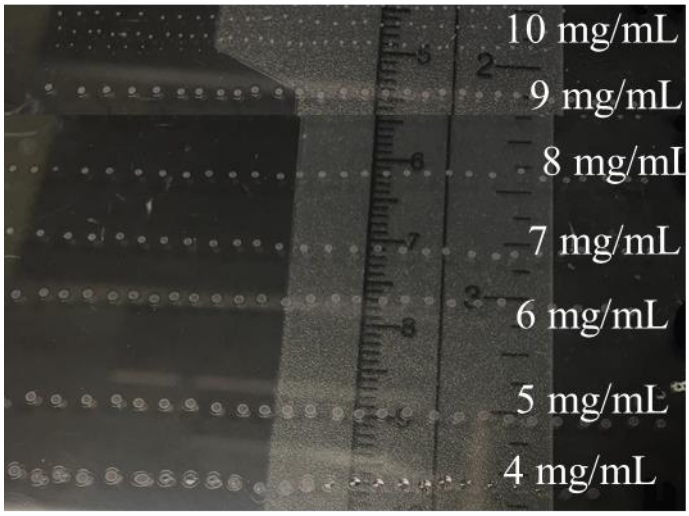

Figure 3.10 Matrigel droplets with concentrations ranging from 4 mg/mL to 10 mg/mL.

In each case, Matrigel provided a stable environment for the cells without drying (measured for up to 10 minutes) with longer times when printed closely together as would be in a scaffold. As the filament width of the scaffolds was measured between 400 to 500 µm, a Matrigel concentration of 9 mg/mL was selected to be appropriate for generating droplets which could be deposited on top of the filaments. Approximately $1x10^6$ cells suspended in PBS were pipetted in Matrigel. Immediately before printing, the hASCs+Matrigel bio-ink was transferred to a 160 µm nozzle tip that had been kept on ice.

The ideal parameters for dispensing hASCs+Matrigel bio-ink droplets were investigated. Parameters including distance of the nozzle tip from glass slide, dispensing time of droplet, and air pressure were varied (Table 3.2).

Table 3.2 Experimental set-up to determine hASC + Matrigel printing parameters.

Distance from Substrate (µm)	Dispensing Time (ms)	Air Pressure (psi)
100	25	10
200	25	10
100	35	10
200	35	10
100	25	20
200	25	20
100	35	20
200	35	20

Droplets made at higher air pressure (20 psi) only showed the presence of cells in a blue ring (Figure 3.11E-H) indicating that cells are at the boundary of the droplet due to the high pressure irrespective of the other two parameters. Droplets printed at the lower air pressure (10 psi) provide a more uniform distribution of cells, the presence of which are indicated with white arrows (Figure 3.11A-D). An even distribution of cells is ideal when printing to ensure better coverage of the scaffold.

Droplets printed with 10 psi and a height of 200 µm from the substrate had more cells (152±1) in comparison to those printed at 10 psi with a height of 100 µm (127±20). When comparing the pulse time, the droplets printed using 35 ms had a slightly higher cell count than those printed using 25 ms by 3 cells on average. Therefore, the printing parameters for Matrigel droplets were determined to be: (i) air pressure of 10 psi, (ii) distance from glass slide of 200 µm, and (iii) pulse duration of 35 ms. These parameters were used for all subsequent tests with Matrigel droplets.

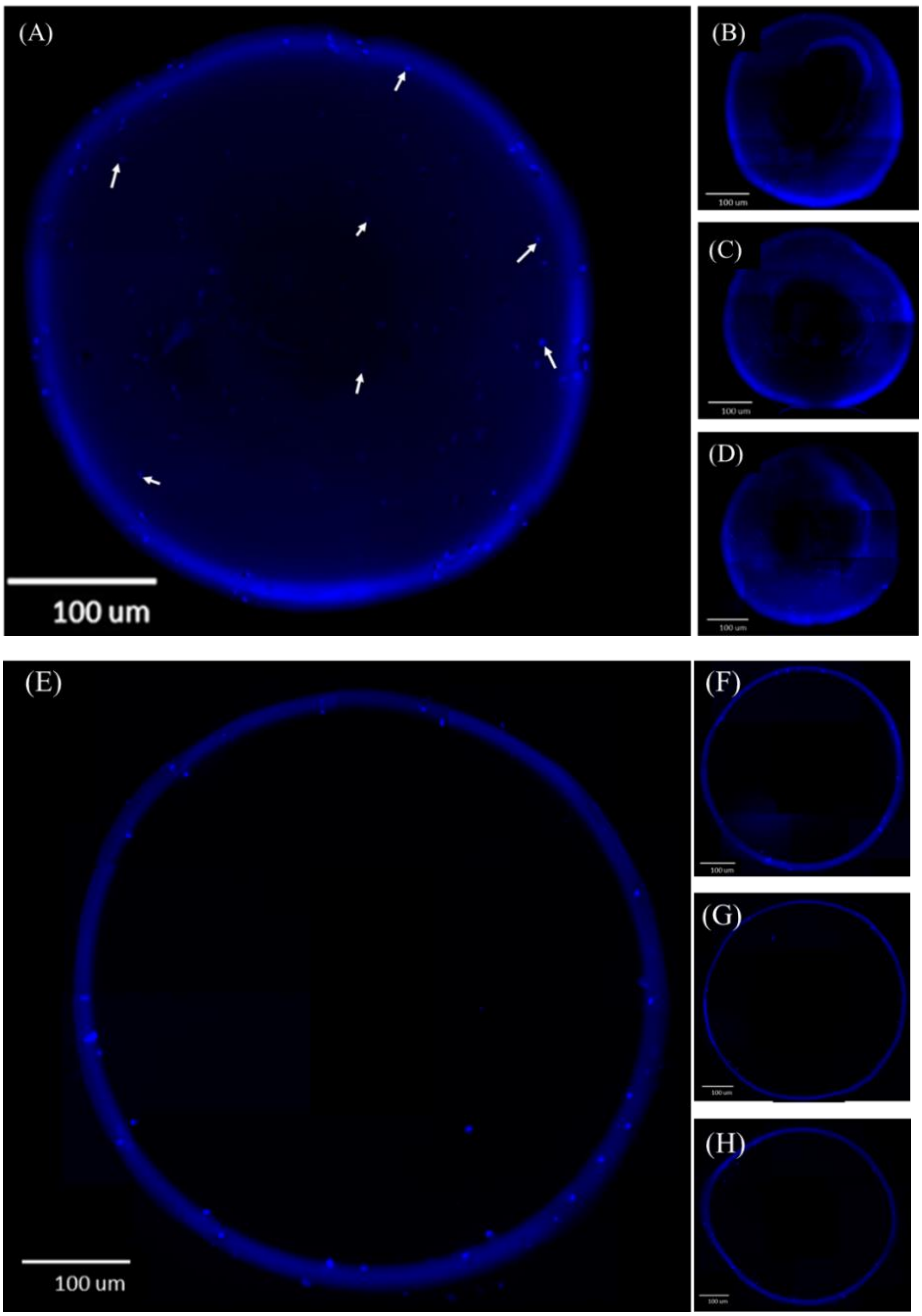

Figure 3.11 DAPI stained fluorescent images of $1x10^6$ hASCs/mL Matrigel printed at (A-D) 10 psi and (E-H) 20 psi. (A,E) A pulse time of 35 ms and 200 µm distance from glass slide (B,F) 25 ms and 200 µm (C,G) 35 m s and 100 µm (D,H) 25 ms and 100 µm. The average number of cells at 10 psi is 127 while the average number at 20 psi is 152. The cells are at the boundary of the droplet for 20 psi because of higher air pressure.

3.5.2. Viability of Stem Cells Printed on Composite Scaffold. The viability of hASCs printed at 10 psi on three layers of the C5 composite was studied by performing a live/dead assay after incubating the samples for 24 hours and 1 week. This was to address the safety issue of using CF while depositing hASCS. The viability of cells after 24 hours was 70±10% (Figure 3.12A and 3.12B) as calculated from 15 representative images of 3 scaffolds. After 1 week, the viability of cells was 58±11% (Figure 3.12C and 3.12D). The cells and the Matrigel appear to be adhering to the scaffold and spreading over the pores after 24 hours (Figure 3.12A).

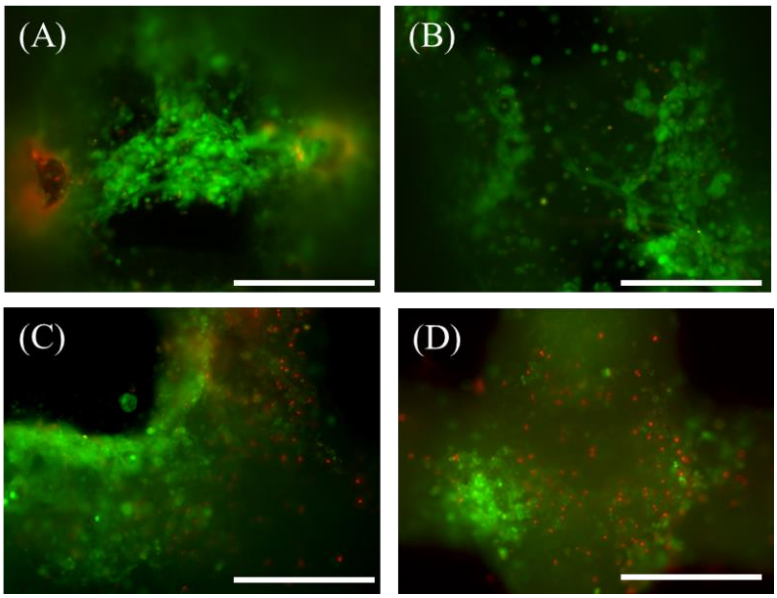

Figure 3.12 Representative Live/Dead images of Matrigel encapsulated ASCs on C5 scaffold. Imaged after (A-B) 24 hours with 70% viability, and (C-D) 1 week with 58% viability. Scale bars - 250 μm.

3.5.3. Matrigel Droplets in Multiple Layer Scaffolds. After printing three layers of the PCL/13-93B3 composite (240 μm thick) with a single layer of Matrigel droplets, the efficacy of this methods with multiple layer scaffolds was investigated. Therefore, 10 layer PCL/13-93B3 scaffolds (800 μm thick) were printed without any

Matrigel and compared to scaffolds with 5 layers of Matrigel droplets printed every two layers (Figure 3.13). The scaffolds could not be printed any thicker due to material build up on the edges causing bridging of the pores. Additionally, some of the scaffolds (about 1 in 4) demonstrated visible warping due to shrinkage stresses (Figure 3.13D).

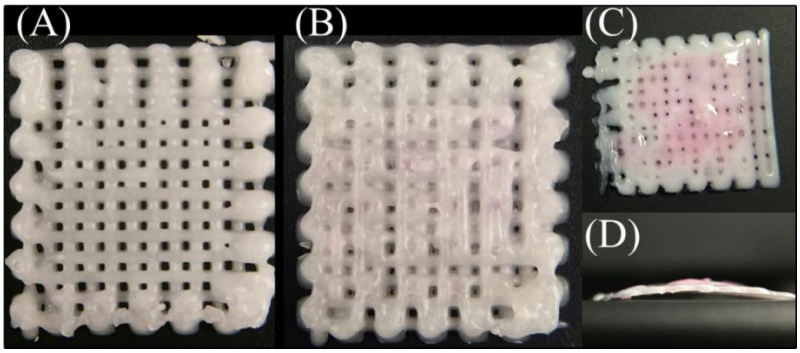

Figure 3.13 C3 scaffolds printed (A) without and (B-C) with Matrigel. (D) Side view of (C) showing warping. Scaffolds are 10x10 mm^2 and 10 layers (800 μm thick). The scaffold in (A) contains no Matrigel while the scaffolds in (B-C) contain 5 layers of Matrigel droplets printed every two layers.

Because the droplets affected the printing of the scaffold, it was decided that further tests would use hydrogel filaments printed between the composite filaments rather than hydrogel droplets (Figure 3.14). The placement of the droplets was not precise enough using the current printer to avoid impeding deposition of the following composite layers over time. In addition, printing hydrogel filaments between the composite filaments could help when trying to fabricate pores in the x and y-direction.

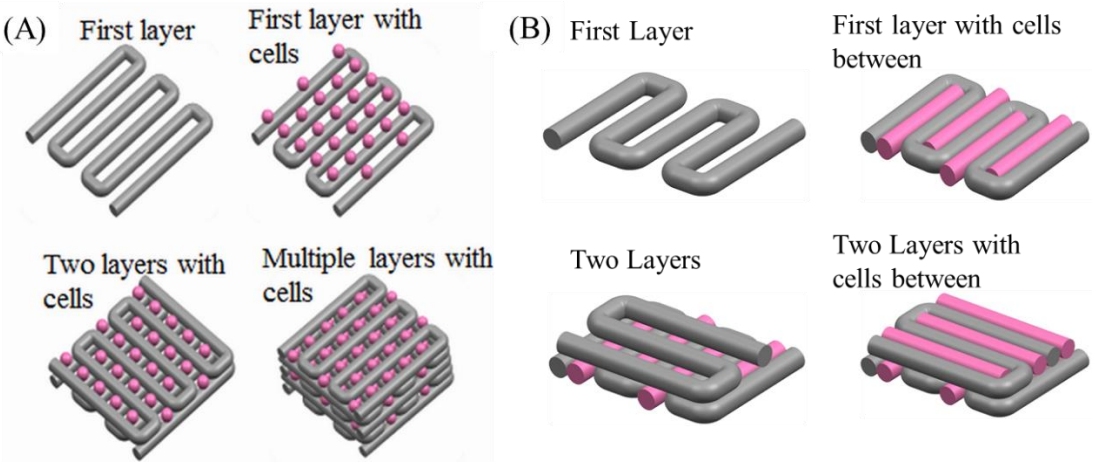

Figure 3.14 Comparison of two printing methods (A) with hydrogel droplets and (B) with hydrogel filaments.

3.6. COMPARE PCL/13-93B3 COMPOSITE TO OTHER BIO-INKS

3.6.1. Without Cells. Single layers were printed for each bio-ink. Parameters for the C3 composite filaments were determined in the previous section. PBS, used as a control to measure cell death through the printing process, had a large amount of spreading when printed even with a 60 μm nozzle and only 2 psi (Figure 3.15A). Increasing the printing speed from 10 mm/s did not produce more consistent filament size and shape. Pluronic (15% w/v) and Matrigel filaments (4.5 mg/mL) had similar properties. Both required a 160 μm nozzle and were printed at 2 psi and 10 mm/s (Figure 3.15B and 3.15C). Any larger nozzle or higher pressure and the hydrogel spread such that there was no longer space between the printed filaments and instead there was just a puddle. A smaller nozzle (<160 μm) and decreased pressure (<2 psi) did not print consistently and produced filaments that were not continuous. A filament spacing of 1 mm was required for the PBS, Matrigel, and Pluronic to prevent the filaments overlapping while the composite could be printed with 800 μm spacing.

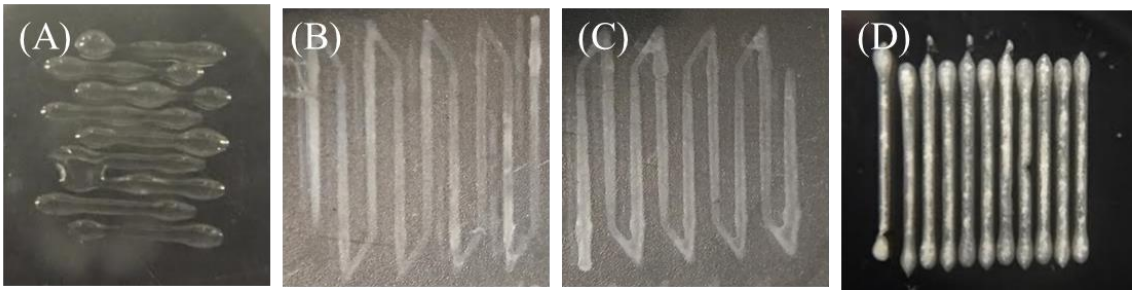

Figure 3.15 Macroscopic images of (A) PBS, (B) Matrigel, (C) Pluronic, and (D) C3 Composite. Images were taken within 5 minutes of printing.

3.6.2. With Cells. Approximately $5x10^6$ rBMSCs/mL were suspended in C3 paste, Matrigel, Pluronic, and PBS. One layer was printed of each bio-ink and they were incubated in cell culture conditions for 1 day and 1 week. The majority of the rBMSCs in the pluronic and Matrigel are noticeably suspended after one day while after 1 week there is a mix of suspended rBMSCs and adhered rBMSCs exhibiting a fibroblast-like morphology integral to MSCs (Figure 3.16B and 3.16C). Using bright field microscopy, no cells can be observed in the composite as the filaments were too dense to image through properly (Figure 3.16D).

Upon examination using a Live/Dead stain and fluorescent microscopy, the composite shows signs of cell survival within the filament both one day and one week after printing with rBMSCs (Figure 3.17). With Matrigel and Pluronic, the cells are mostly in clusters and remain in the filaments in which they were printed after one day Figure 3.17B and 3.17C). After a week, the cells in Matrigel and Pluronic started to spread and adhere to the plate, though some remained suspended (Figure 3.17F and 3.17G). The rBMSCs printed with the PBS show an increased amount of death along the edges of where they were printed both one day and one week after printing (Figure 3.17A and 3.17E). There was no statistical difference between the viability of the cells of each bio-ink both one day and one week after printing indicating no long term negative effects after printing (Figure 3.17I and 3.17J).

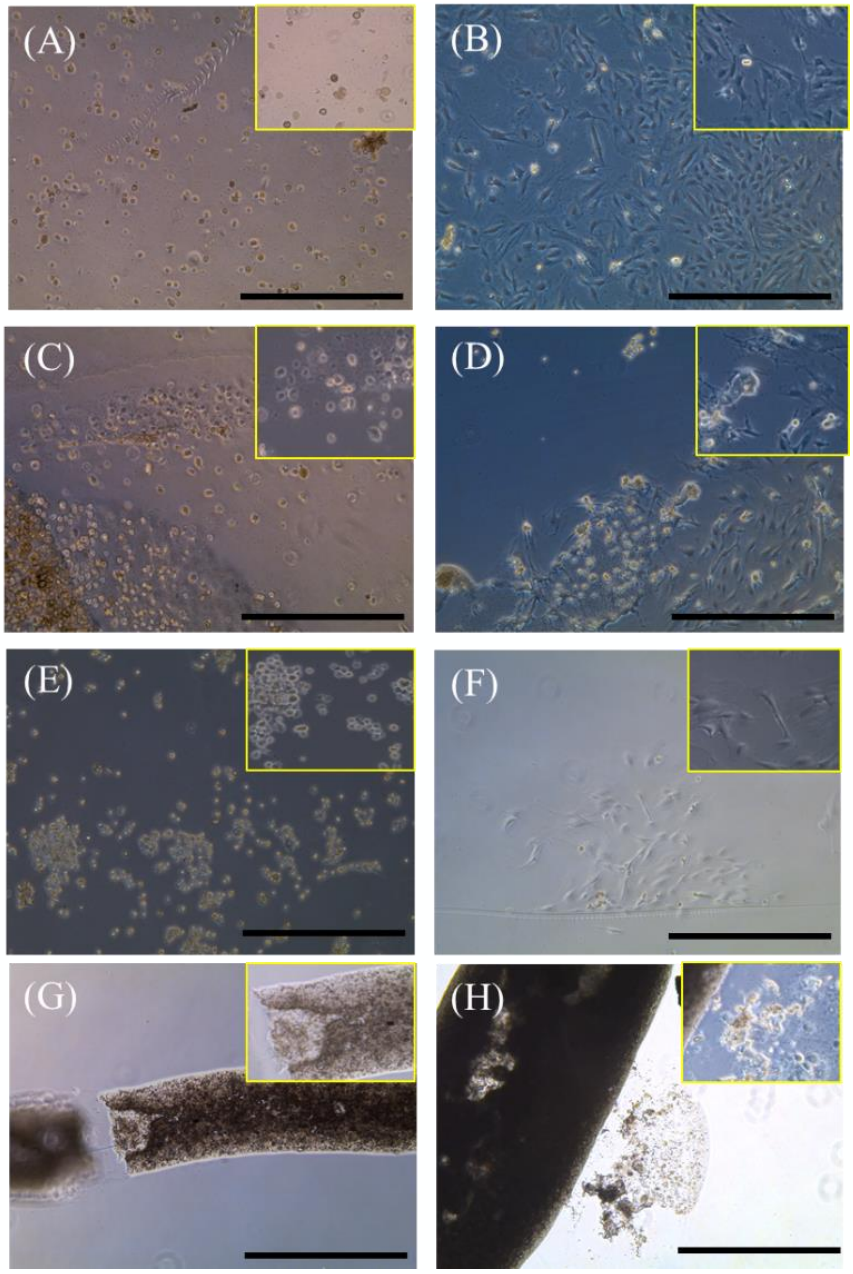

Figure 3.16 Bright field images of rBMSCs after (A,C,E,G) 1 day and (B,D,F,H) 1 week suspended in (A-B) PBS, (C-D) Matrigel (4.5 mg/mL), (E-F) Pluronic (15% w/v), and (G-H) C3 composite. The cells were printed at a concentration of $5x10^6$ per mL. Scale bars - 1 mm.

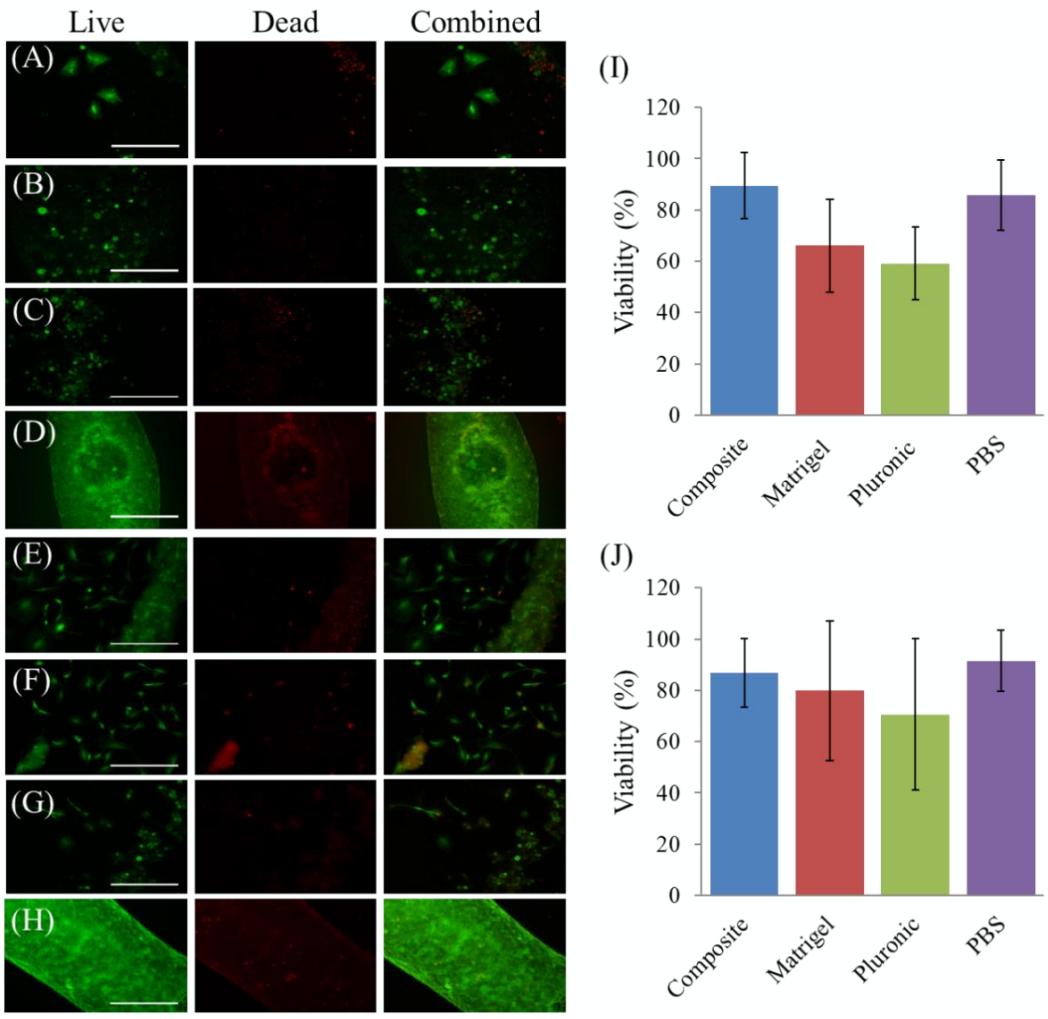

Figure 3.17 Viability of rBMSCs (A-D,I) 1 day and (E-H,J) 1 week after printing suspended in (A,E) PBS, (B,F) Matrigel, (C,G) Pluronic, and (D,H) the C3 composite. No statistical difference in viability between the different bio-inks both (I) 1 day and (J) 1 week after printing. The rBMSCs were suspended at a concentration of $5x10^6$ cells per mL. Scale bars - 250 µm.

3.7. COMPARISON OF DIFFERENT STEM CELL POPULATIONS

3.7.1. Rat SVF. The concentration of cells per mL of bio-ink was investigated using 25% w/v Pluronic with rSVF and rBMSCs. A single layer of Pluronic was printed in a 10x10 mm^2 scaffold. After one day, a live/dead stain shows ~95% cell death for the rSVF at all concentrations (Figure 3.18A-C). It was also noticed that the Pluronic did not

remain in distinct filaments after the media was added. Most likely, this was due to the media being too cold when added, causing the Pluronic to dissolute. A high degree of cell death is expected with SVF as it contains many different cell types and the culture media (D-10) is specific just to MSCs. Therefore, the experiment was repeated with rBMSCs with $5x10^6$ and $10x10^6$ cells. However, once again there was about 96% cell death after one day (Figure 3.18D-E). The large amount of cell death after one day using both rSVF and rBMSCs suggests that 25% w/v Pluronic is not ideal for cell survival.

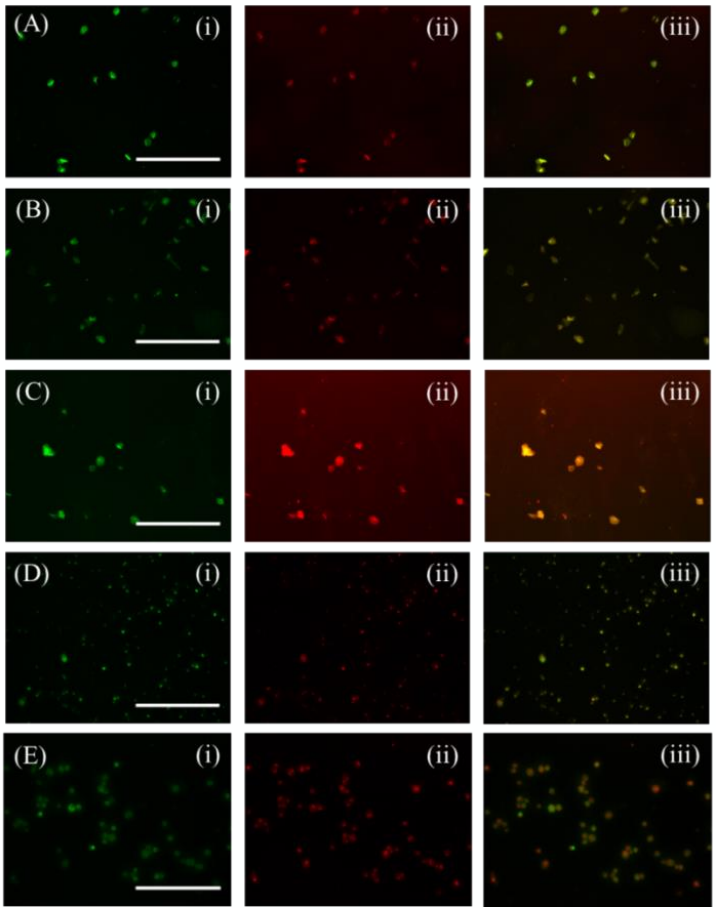

Figure 3.18 Live/Dead images of cells suspended in 25% w/v Pluonic at (A) $5x10^6$, (B) $10x10^6$, and (C) $20x10^6$ rSVF per mL and (D) $5x10^6$ and (E) $10x10^6$ rBMSCs per mL. The images are the (i) live cells, (ii) dead cells, and (iii) a combined image of live and dead cells. All show <5% viability. Scale bars - 250 µm.

Despite the problems encountered using rSVF previously, the positive results from different bio-inks using rBMSCs prompted a trial with rSVF. Approximately $5x10^6$ rSVF/mL of bio-ink was suspended in PBS, Matrigel (4.5 mg/mL), Pluronic (15% w/v) and the C3 composite. One layer of each bio-ink was printed and scaffolds were incubated in cell culture conditions for one day. The results show a distinct lack of cells via both bright field and fluorescent imaging (Figure 3.19). A large amount of cell death is expected within the first 24 hours for SVF due to the variety of cell types and the culture media being optimized for only MSCs. Therefore, it was concluded that a live/dead analysis could not be performed after one day.

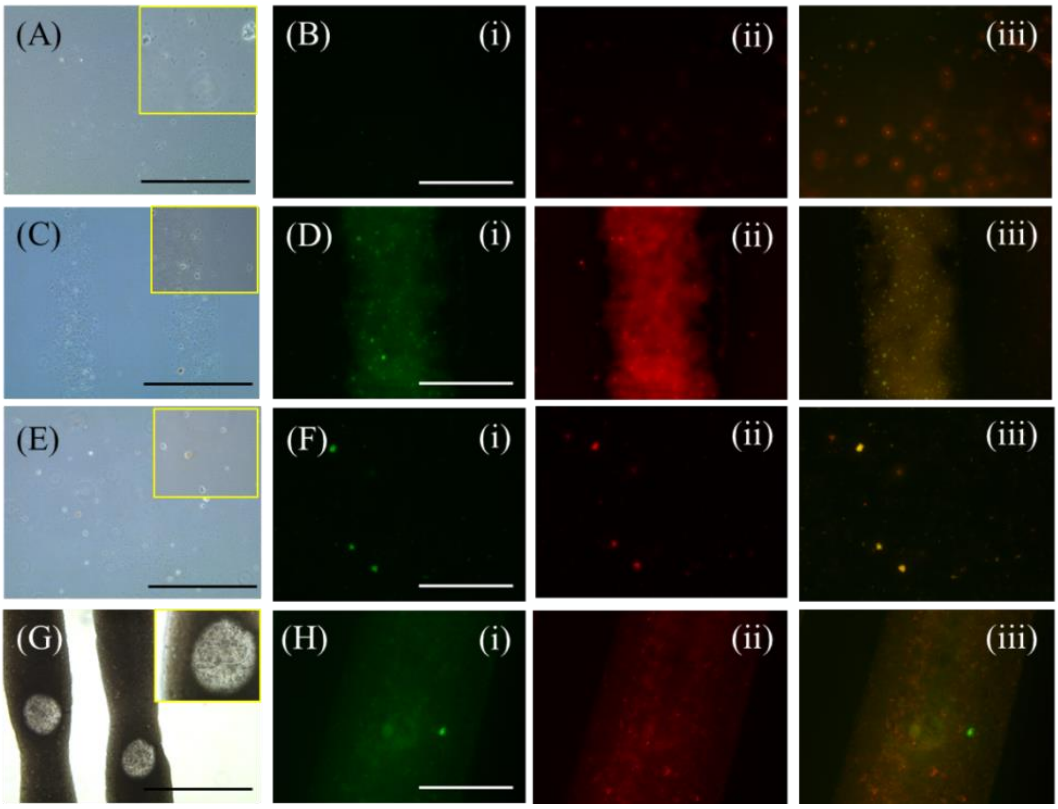

Figure 3.19 (A,C,E,G) Bright field and (B,D,F,H) live/dead images one day after printing rSVF suspended in (A-B) PBS, (C-D) Matrigel (4.5 mg/mL), (E-F) Pluronic (15% w/v), and (G-H) C3 composite. The cells were printed at a concentration of $5x10^6$ per mL and had <5% viability for all bio-inks. The images are the (i) live cells, (ii) dead cells, and (iii) a combined image of live and dead cells. The scale bars on the bright field images are 1 mm while the fluorescent images are 250 µm.

3.7.2. Human Cells. A mixture of $5x10^6$ hASCs and hBMSCs was suspended in the different bio-inks, printed, and analyzed after one day using a live/dead stain and bright field microscopy (Figure 3.20). Matrigel (4.5 mg/mL) and Pluronic (15% w/v) both had a mixture of cells staying suspended in the hydrogel as well as cells showing a fibroblast-like morphology (Figure 3.20B and 3.20C). The cells printed in Pluronic are similar to the PBS control in that they started showing directional growth (Figure 3.20A and 3.20C). The composite shows signs of cell survival within the filaments as well (Figure 3.20D). Each bio-ink showed greater than 96% viability.

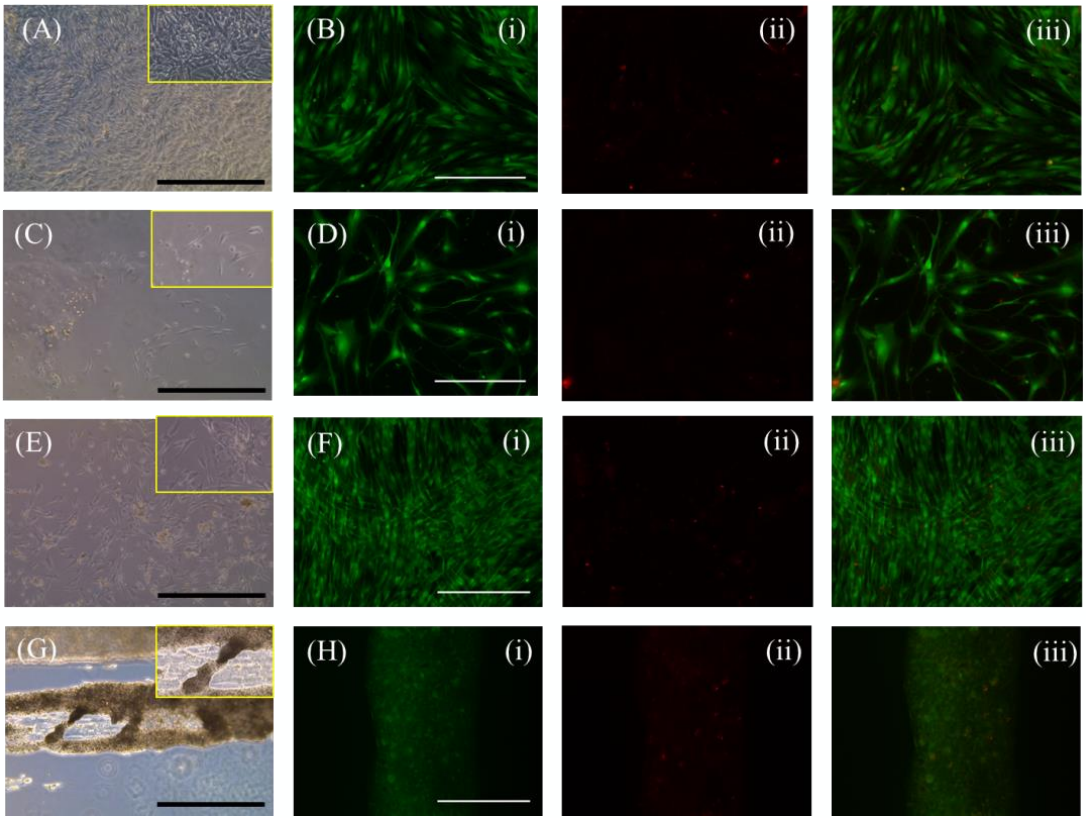

Figure 3.20 (A,C,E,G) Bright field and (B,D,F,H) live/dead images one day after printing hASCs and hBMSCs suspended in (A,B) PBS, (C,D) Matrigel (4.5 mg/mL), (E,F) Pluronic (15% w/v), and (G,H) C3 composite. The cells were printed at a concentration of $5x10^6$ per mL. The images are the (i) live cells, (ii) dead cells, and (iii) a combined image of live and dead cells. The scale bars on the bright field images are 1 mm while the fluorescent images are 250 µm.

3.7.3. Viability. The viability of the different stem cell populations was compared after one day for all bio-inks. A low viability was seen for all cell types and concentrations in the 25% w/v Pluronic while there was low and inconsistent viability of the rSVF in all bio-inks (Figure 3.21). For all bio-inks, the rBMSCs had an average viability of 60% or higher while the hMSCs had an average viability of 80% or higher. However, the only difference between the two statistically is with the 15% w/v Pluronic. From this data, it was concluded that the 25% w/v Pluronic provided unsuitable tissue culture conditions, the viability of rSVF cannot be evaluated after one day, and there is no statistical difference in viability for PBS, Matrigel, 15% w/v Pluronic, and the composite.

3.8. INVESTIGATING THE BEST METHOD TO ANALYZE STEM CELL ACTIVITY AFTER PRINTING CELLS IN DIFFERENT BIO-INKS

After both one day and one week, it can be determined that CyQuant is not a viable option to estimate cell number for the composite (Figure 3.22C-D). Approximately 4.5-7x10^4 cells were printed per scaffold and almost no cells were measured in the composite after one day. After one day, the assay detected approximately 1/10 of the cells printed in Matrigel and Pluronic and ~1/2 the cells printed in PBS. Matrigel showed a six-fold increase in cell number after one week while the Pluronic has a ten-fold increase, which indicates the cells are surviving and proliferating. Surprisingly, the MTT assay exhibited a decrease in absorbance, which is equated with percent viability, after one week for all bio-inks (Figure 3.22A and 3.22B). This is inconsistent with the results from the live/dead analysis that show similar viability from one day to one week (Figure 3.17I and 3.22J). This could be due to problems when transferring to the 96-well plate but the MTT assay does not seem to be a viable option as a high through put assay to analyze the composite scaffolds. The composite scaffolds returned unusally high absorbance numbers with a high standard deviation that suggest the composite itself interferes with the assay (Figure 3.22A and 2.32B). The high standard deviations and odd decrease in absorbance

after one week suggest that an additional trial would need to be run to make further conclusions on the efficacy of using this method to analyze the other bio-inks.

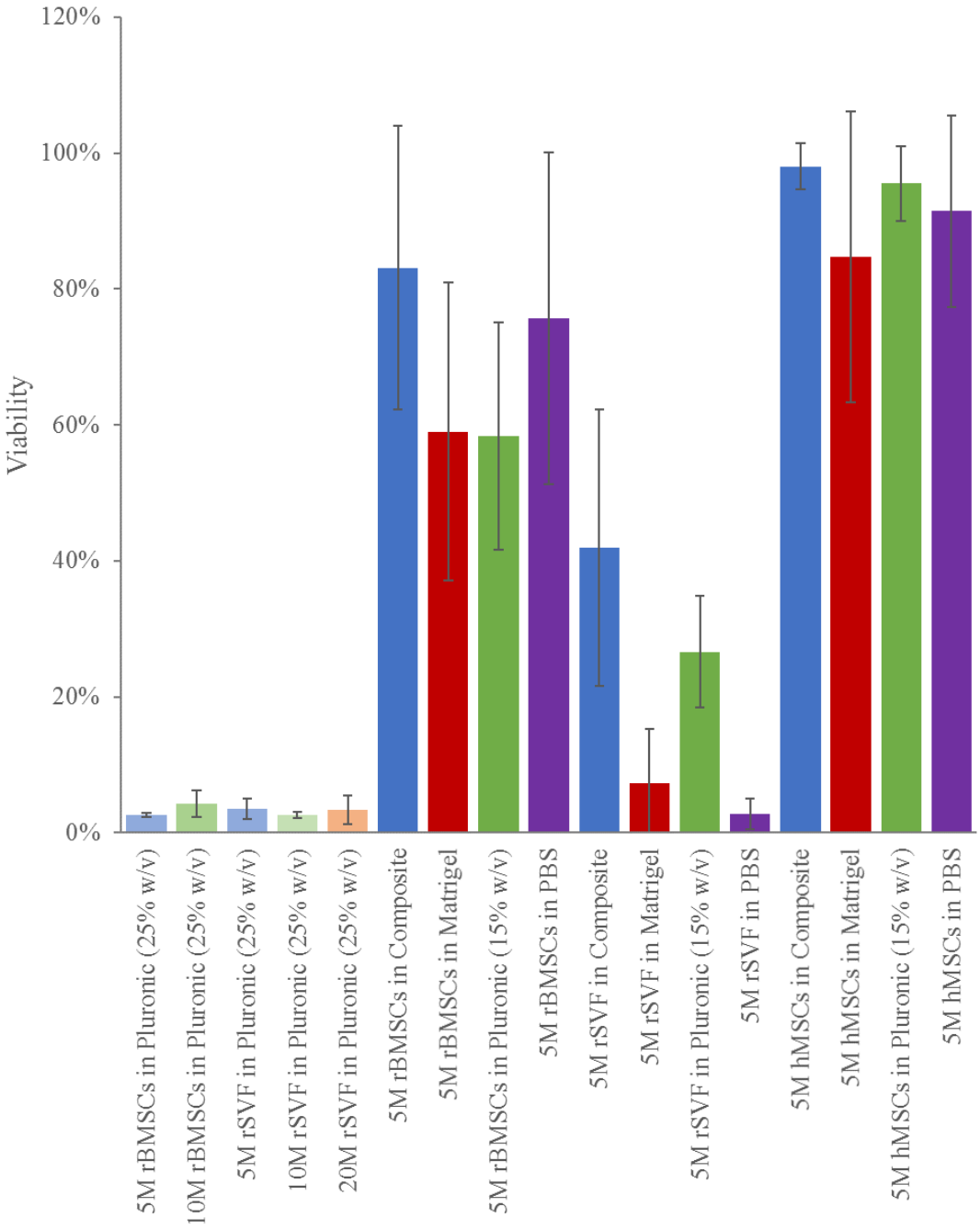

Figure 3.21 Viability of different cell types in all bio-inks after one day.

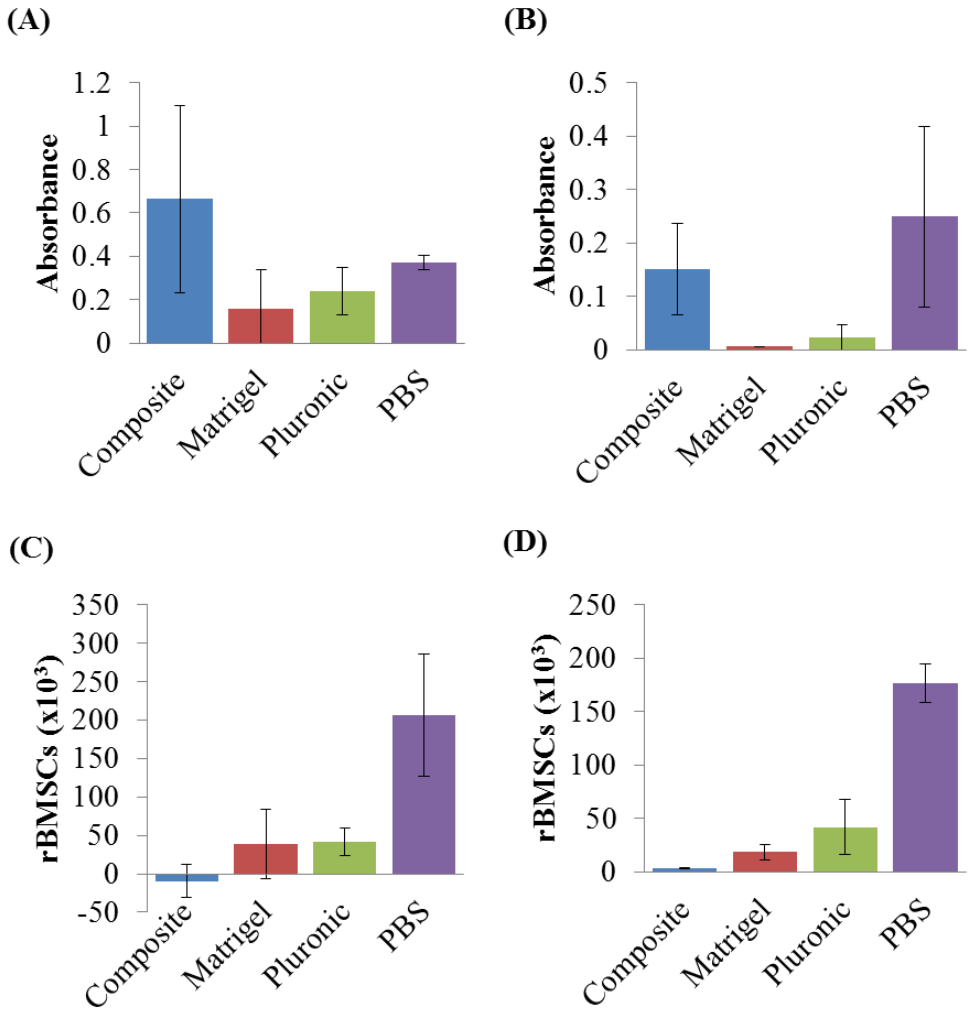

Figure 3.22 Methods to evaluate bio-printed rBMSCs, (A-B) Viability and (C-D) number of rBMSCs (A,C) 1 day and (B,D) 1 week after printing. There was no significant difference between the Matrigel and Pluronic. The results are inconsistent for the C3 composite and indicate the unsuitability of these particular tests when determining viability and cell number. The cells were printed at a concentration of $5x10^6$ cells per mL.

4. CONCLUSION

Printing parameters for different glass concentrations of a chloroform-dissolved PCL/13-93B3 glass composite were established using a modified extrusion printer. Scaffolds with no warpage were fabricated using 30-50wt.% glass. Scaffolds exhibited bioactivity through a controlled release of bioactive glass in media over two weeks and the formation of hydroxyapatite-like crystals on the surface. This demonstrates that bioactive glass can be printed without the need to heat up to hundreds of degrees centigrade, making it possible to print cells concurrently on the scaffold.

The effect of chloroform evaporation on cell viability was determined by printing droplets of hASCs suspended in Matrigel on a single layer of the composite paste. One week after printing and incubating under standard cell culture conditions, more than 60% hASCs were shown to be viable. With multi-layer scaffolds, the droplets could not be precisely placed such that they did not interfere with printing the next layer of the composite. This caused the scaffolds to print inconsistently and fill in the pores which indicates that although cells can survive the printing and choice of biomaterials, they need to be printed with a different method in order to maintain the integrity of the scaffold.

The ability of cells to be printed in different bio-inks as filaments and not droplets was evaluated. MSCs were suspended in the composite, Matrigel, and Pluronic hydrogel then printed in a single layer and incubated under standard cell culture conditions for one day and one week. Matrigel and Pluronic had a mix of rBMSCs both suspended and exhibiting spreading behavior after one week while PBS only had spreading cells. The viability of all the bio-inks after both one day and one week as measured using a live/dead assay was over 60%. There was no significant difference between the viability of the different bio-inks, which means using the composite as a bio-ink is feasible

Different sources of MSCs were printed to evaluate the ideal cell type for bioprinting. One day after printing, a mixture of hASCs and hBMSCs had a viability of over 96% in all bio-inks. The cells suspended in PBS and Pluronic even showed directional growth typical of spreading MSCs while the cells suspended in Matrigel showed fibroblast-like morphology. This is in comparison to rBMSCs which had over

60% viability and fibroblast-like morphology in PBS, Pluronic, and Matrigel. rSVF was investigated as a possible source; however, evaluation should not be performed after one day.

In order to determine the best method to measure cellular activity after printing, different biological assays were evaluated. The composite, Matrigel, and Pluronic were evaluated at 1 day and 1 week after printing using a MTT assay, CyQuant assay, and a Live/Dead stain. The MTT and CyQuant assays were unable to accurately detect cells within the composite leaving the Live/Dead stain as the best method to evaluate cell numbers and viability.

Future directions include evaluating different MSC populations on a multiple layer scaffold for both viability and differentiation capacity. Another direction would be investigating the use of different polymers and solvents and their uses for applications besides bone.

REFERENCES

1. United States Bone and Joint Initiative. *The Burden of Musculoskeletal Diseases in the United States*. (American Academy of Orthopaedic Surgeons, 2011).

2. Bohner, M. Resorbable biomaterials as bone graft substitutes. *Mater. Today* **13,** 24–30 (2010).

3. Moore, W. R., Graves, S. E. & Bain, G. I. Synthetic bone graft substitutes. *ANZ J. Surg.* **71,** 354–361 (2001).

4. Gamie, Z. *et al.* Stem cells combined with bone graft substitutes in skeletal tissue engineering. *Expert Opin. Biol. Ther.* **12,** 713–729 (2012).

5. Li, M. T. A., Willett, N. J., Uhrig, B. A., Guldberg, R. E. & Warren, G. L. Functional Analysis of Limb Recovery following Autograft Treatment of Volumetric Muscle Loss in the Quadriceps Femoris. *J. Biomech.* **47,** 2013–2021 (2014).

6. Mariscalco, M. W. *et al.* Autograft versus nonirradiated allograft tissue for anterior cruciate ligament reconstruction: A systematic review. *Am. J. Sports Med.* **42,** 492–499 (2014).

7. Shrivats, A. R., McDermott, M. C. & Hollinger, J. O. Bone tissue engineering: State of the union. *Drug Discovery Today* (2014). doi:10.1016/j.drudis.2014.04.010

8. Oryan, A., Alidadi, S., Moshiri, A. & Maffulli, N. Bone regenerative medicine: classic options, novel strategies, and future directions. *J. Orthop. Surg. Res.* (2014). doi:10.1186/1749-799X-9-18

9. Nguyen, L. H. *et al.* Vascularized bone tissue engineering: Approaches for potential improvement. *Tissue Eng. - Part B Rev.* **18,** 363–382 (2012).

10. Orlando, G. *et al.* Regenerative medicine as applied to solid organ transplantation: Current status and future challenges. *Transplant International* (2011). doi:10.1111/j.1432-2277.2010.01182.x

11. Guillotin, B. *et al.* Laser assisted bioprinting of engineered tissue with high cell density and microscale organization. *Biomaterials* **31,** 7250–7256 (2010).

12. Yan, J. *et al.* Laser-assisted printing of alginate long tubes and annular constructs. *Biofabrication* **5,** 15002 (2013).

13. Chang, C. C., Boland, E. D., Williams, S. K. & Hoying, J. B. Direct-write bioprinting three-dimensional biohybrid systems for future regenerative therapies. *J. Biomed. Mater. Res. - Part B Appl. Biomater.* **98B,** 160–170 (2011).

14. Ozbolat, I. T. & Hospodiuk, M. Current advances and future perspectives in extrusion-based bioprinting. *Biomaterials* **76,** 321–343 (2016).

15. Rengier, F. *et al.* 3D printing based on imaging data: Review of medical applications. *International Journal of Computer Assisted Radiology and Surgery* (2010). doi:10.1007/s11548-010-0476-x

16. Hoque, M. E., Chuan, Y. L. & Pashby, I. Extrusion based rapid prototyping technique: An advanced platform for tissue engineering scaffold fabrication. *Biopolymers* (2011). doi:10.1002/bip.21701

17. Ulery, B. D., Nair, L. S. & Laurencin, C. T. Biomedical applications of biodegradable polymers. *J. Polym. Sci. Part B Polym. Phys.* **49,** 832–864 (2011).

18. Woodruff, M. A. & Hutmacher, D. W. The return of a forgotten polymer—Polycaprolactone in the 21st century. *Prog. Polym. Sci.* **35,** 1217–1256 (2010).

19. Puska, M., J., A. & Vallittu, P. in *Advances in Composite Materials - Analysis of Natural and Man-Made Materials* (InTech, 2011). doi:10.5772/20657

20. Temple, J. P. *et al.* Engineering anatomically shaped vascularized bone grafts with hASCs and 3D-printed PCL scaffolds. *J. Biomed. Mater. Res. - Part A* **102,** 4317–4325 (2014).

21. Handel, M., Hammer, T. R., Nooeaid, P., Boccaccini, A. R. & Hoefer, D. 45S5-bioglass(R)-Based 3D-scaffolds seeded with human adipose tissue-derived stem cells induce in vino vascularization in the CAM angiogensis assay. *Tissue Eng. - Part A* **19,** 2703–2712 (2013).

22. Rath, S. N. *et al.* Adipose- and bone marrow-derived mesenchymal stem cells display different osteogenic differentiation patterns in 3D bioactive glass-based scaffolds. *J. Tissue Eng. Regen. Med.* (2016). doi:10.1002/term.1849

23. Rahaman, M. N. *et al.* Bioactive glass in tissue engineering. *Acta Biomater.* **7,** 2355–2373 (2011).

24. Jung, S. B. & Day, D. E. Revolution in wound care? Inexpensive, easy-to-use cotton candy-like glass fibers appear to speed healing in initial venous stasis wound trial. *Am. Ceram. Soc. Bull.* **90,** 25–29 (2011).

25. Lin, Y., Brown, R. F., Jung, S. B. & Day, D. E. Angiogenic effects of borate glass microfibers in a rodent model. *J. Biomed. Mater. Res. - Part A* **102,** 4491–4499 (2014).

26. Korpela, J. *et al.* Biodegradable and bioactive porous scaffold structures prepared using fused deposition modeling. *J. Biomed. Mater. Res. - Part B Appl. Biomater.* **101,** 610–619 (2013).

27. Miller-Chou, B. A. & Koenig, J. L. A review of polymer dissolution. *Progress in Polymer Science (Oxford)* 28 (2003). doi:10.1016/S0079-6700(03)00045-5

28. Mohammadkhah, A., Marquardt, L. M., Sakiyama-Elbert, S. E., Day, D. E. & Harkins, A. B. Fabrication and characterization of poly-(ε)-caprolactone and bioactive glass composites for tissue engineering applications. *Mater. Sci. Eng. C* **49,** 632–639 (2015).

29. Salem, H. K. & Thiemermann, C. Mesenchymal stromal cells: Current understanding and clinical status. *Stem Cells* **28,** 585–596 (2010).

30. Wu, Y., Chen, L., Scott, P. G. & Tredget, E. E. Mesenchymal Stem Cells Enhance Wound Healing Through Differentiation and Angiogenesis. *Stem Cells* **25,** 2648–2659 (2007).

31. De Ugarte, D. A. *et al.* Comparison of multi-lineage cells from human adipose tissue and bone marrow. *Cells Tissues Organs* **174,** 101–109 (2003).

32. Izadpanah, R. *et al.* Biologic properties of mesenchymal stem cells derived from bone marrow and adipose tissue. *J. Cell. Biochem.* **99,** 1285–1297 (2006).

33. Wagner, W. *et al.* Comparative characteristics of mesenchymal stem cells from human bone marrow, adipose tissue, and umbilical cord blood. *Exp. Hematol.* **33,** 1402–1416 (2005).

34. Sakaguchi, Y., Sekiya, I., Yagishita, K. & Muneta, T. Comparison of human stem cells derived from various mesenchymal tissues: Superiority of synovium as a cell source. *Arthritis Rheum.* **52,** 2521–2529 (2005).

35. D'Andrea, F. *et al.* Large-Scale Production of Human Adipose Tissue from Stem Cells: A New Tool for Regenerative Medicine and Tissue Banking. *Tissue Eng. - Part C Methods* **14,** 233–242 (2008).

36. Casteilla, L. & Dani, C. Adipose tissue-derived cells: From physiology to regenerative medicine. *Diabetes Metab.* **32,** 393–401 (2006).

37. Riordan, N. H. *et al.* Non-expanded adipose stromal vascular fraction cell therapy for multiple sclerosis. *J. Transl. Med.* **7,** 29 (2009).

38. Bourin, P. *et al.* Stromal cells from the adipose tissue-derived stromal vascular fraction and culture expanded adipose tissue-derived stromal/stem cells: A joint statement of the International Federation for Adipose Therapeutics and Science (IFATS) and the International So. *Cytotherapy* **15,** 641–648 (2013).

39. Obara, C. *et al.* Characteristics of three-dimensional prospectively isolated mouse bone marrow mesenchymal stem/stromal cell aggregates on nanoculture plates. *Cell Tissue Res.* (2016). doi:10.1007/s00441-016-2405-y

40. Mohammadi, R. *et al.* Repair of nerve defect with chitosan graft supplemente uncultured characterized stromal vascular fraction in streptozotocin induced diabetic rats. *Int. J. Surg.* (2014). doi:10.1016/j.ijsu.2013.10.018

VITA

Caroline Blair Murphy matriculated at Missouri S&T in the fall of 2011 and pursued a Bachelor's Degree in Ceramic Engineering and graduated in May 2015. That fall, she re-enrolled as a Mechanical Engineering Master's student, and completed her Master of Science Degree in July 2017.